

11945-6051

000000 111 43

Quantifying BRDF Effects in Comparing Landsat-7 and AVIRIS Near-Simultaneous
Acquisitions for Studies of High Plains Vegetation Cover

A. F. H. Goetz^{1,2,*}, K. B. Heidebrecht¹, E.D. Gutmann^{1,2}, A.S. Warner^{1,2},
E. L. Johnson¹, L. R. Lestak¹

¹Center for the Study of Earth from Space, CIRES
and ²Department of Geological Sciences
University of Colorado, Boulder, CO
USA

Abstract

Approximately 100,000 sq. km of the High Plains of the central United States are covered by sand dunes and sand sheets deposited during the Holocene. Soil-dating evidence shows that there were at least four periods of dune reactivation during major droughts in the last 10,000 years. The dunes in this region are anchored by vegetation. We have undertaken a study of land-use change in the High Plains from 1985 to the present using Landsat 5 TM and Landsat 7 ETM+ images to map variation in vegetation cover during wet and dry years. Mapping vegetation cover of less than 20% is important in modeling potential surface reactivation since at this level the vegetation no longer sufficiently shields sandy surfaces from movement by wind.

Landsat TM data have both the spatial resolution and temporal coverage to facilitate vegetation cover analysis for model development and verification. However, there is still the question of how accurate TM data are for the measurement of both growing and senescent vegetation in arid and semi-arid regions. AVIRIS provides both high spectral resolution as well as high signal-to-noise ratio and can be used to test the accuracy of Landsat TM and ETM+ data. We have analyzed data from AVIRIS flown nearly concurrently with a Landsat 7 overpass. The comparison between an AVIRIS image swath of 11 km width subtending a 30° angle and the same area covered by a 0.8° angle from Landsat required accounting for the BRDF. A normalization technique using the ratio of the reflectances from registered AVIRIS and Landsat data proved superior to the techniques of column averaging on AVIRIS data alone published previously by Kennedy et al (1997). This technique can be applied to aircraft data covering a wider swath angle than AVIRIS to develop BRDF responses for a wide variety of surfaces more efficiently than from ground measurements.

*Address Correspondence to A.F.H. Goetz, University of Colorado at Boulder, CIRES/CSES, Campus Box 216, Boulder, CO 80309-0216, Phone: 303-492-5086, Fax: 303-492-5070, email: goetz@cses.colroad.edu

Introduction

Approximately 100,000 sq. km of the High Plains of the central United States are covered by sand dunes and sand sheets, deposited since the end of the last ice age. In the last 10,000 years, soil dating evidence shows that there were episodic droughts leading to reactivation of sandy soil surfaces, the last of which was approximately 900 years ago (Ahlbrandt et al., 1983; Forman et al, 1992; Muhs et al., 1996). In many areas the sands are dry-farmed for wheat, corn, sorghum and sunflowers. Other areas are used as rangeland. We have undertaken a study of land-use change in the High Plains from 1985 to the present using Landsat 5 TM and Landsat 7 ETM+ images to map variation in vegetation cover during wet and dry years.

The Holocene dunes and sand sheets in the High Plains are currently stabilized by vegetation that reduces surface wind velocities below that required for saltation (Ahlbrandt, 1983). On the High Plains, wind velocities often exceed the 4.8 m/s necessary to initiate movement of bare sandy surfaces. When modeling to predict potential surface reactivation, it is important to map vegetation cover of less than 20%. Buckley (1987) has shown that below 20% cover a wind velocity of 10 m/s at 0.5 m height will begin to move sand, and that at 9% cover the sand transport rate is 65% of the bare sand rate.

In northeastern Colorado (fig. 1) there exist several extensive dune fields with sand derived from the South Platte River during the Holocene. The surfaces consist of single and sometimes overlapping parabolic dunes that trend southeast, consistent with

prevailing winds from the northwest. During the mid- to late Holocene, paleoclimatic data suggest that extensive droughts removed the stabilizing vegetation cover and facilitated sand movement (Woodhouse and Overpeck, 1998). Stratigraphic evidence in northeastern Colorado document extensive, regional eolian sand deposition around 6 ka (Jorgenson, 1992). The key to stability of surfaces is vegetation cover, both above ground and in the anchoring root systems below ground. The 1930's drought, while severe in its effect on the population and farming in the central High Plains, pales in comparison with the mid- to late Holocene climatic conditions. The 1930's dust bowl conditions were not severe enough to kill off much of the natural vegetation cover and, as a consequence, the sand dunes and sand sheets experienced only minor reactivation (Muhs, 1998). Most of the dust and sand that was transported came from tilled fields without any surface cover (Wunder, 1999).

In an ongoing study to model the potential effects of a severe drought in the High Plains, we have concentrated our efforts on determining the potential of Landsat TM data to provide accurate information on vegetation cover, both standing and dead, in the sparsely-vegetated, sandy soils regions (fig. 2). Landsat TM data have both the spatial resolution and temporal coverage to facilitate vegetation cover analysis. However, there is still the question of how accurate TM data are for the measurement of both growing and senescent vegetation in arid and semi-arid regions. AVIRIS provides both high spectral resolution as well as high signal-to-noise ratio and can be considered capable of providing as much information as is currently available on surface conditions from optical remote sensing. Therefore, we undertook to examine a nearly-simultaneously

acquired set of Landsat 7 and AVIRIS (Airborne Visible/Infrared Imaging Spectrometer) data (Green et al, 1998), along with field spectral measurements, to determine the extent to which the two image data sets can provide quantitative information on the amount of photosynthetic vegetation and non-photosynthetic vegetation covering the surface. This paper addresses the question of reconciling measurements made by these diverse sensors.

Because AVIRIS scans $\pm 15^\circ$ about nadir, bi-directional reflectance distribution function (BRDF) effects will cause variations in the apparent reflectance of surface materials depending on their location cross-track in the scene (Deering, 1989). In order to develop an objective comparison with Landsat TM data, AVIRIS data must be corrected for BRDF effects. In this paper, we followed the techniques of Kennedy et al (1997) and made a further advance by making use of Landsat 7 data to normalize the AVIRIS scenes since the AVIRIS swath width only subtends 0.8° in the TM data. We tested this step by using two AVIRIS passes separately, one within 8° of the solar azimuth, to determine the effect of normalization in mapping sparse vegetation cover across an AVIRIS image and to provide a measure of BRDF over the full spectral range of AVIRIS.

Background

Comparison of airborne and spaceborne-acquired image data requires correction for the BRDF effects caused by differing scan geometries and flight trajectories with respect to the solar azimuth between the sensors (Diner et al, 1999; Deering et al, 1991; Middleton et al, 1987). Both theoretical approaches (Kimes, 1983; Irons et al, 1992) and empirical methods (Irons and Labovitz, 1982; Kennedy et al, 1997) can be applied.

Kennedy et al (1997) developed empirical methods to compensate for cross-scan gradients in AVIRIS data over a forested region in Oregon and tested four models, both multiplicative and additive. Their intent was to apply corrections to AVIRIS image data, taken nearly perpendicular to the solar azimuth, that would preserve subtle spectral reflectance features that could be used for foliar chemistry analysis. The brightness gradients observed in airborne and spaceborne images that scan through significant angles about nadir are a combination of a multiplicative BRDF and an additive path radiance effect (Irons et al., 1991). Kennedy et al (1997) addressed this question by calculating column means in each of the 154 band images and for each band, plotting the standard deviation for each column against the mean. A least-squares regression line was fitted to each set of 614 data points. A positive slope with zero intercept indicated a multiplicative or surface BRDF-imposed brightness gradient, while a zero slope with nonzero intercept implied an additive or atmosphere-imposed gradient. Kennedy et al (1997) found both additive and multiplicative behavior and that it was wavelength dependent. However, by first classifying the surface cover type they found strong differences in response to view angle changes among classes that pointed to the BRDF of the surface as the dominant factor causing the view angle-brightness effects.

The AVIRIS data from two flight lines near Brush and Roggen in eastern Colorado in this study differed from the Oregon data (Kennedy et al, 1997) in several respects. The Colorado data were taken over dry-farmed and irrigated row crops and short-grass-prairie rangeland rather than forest. While the Oregon site contained mature and old-growth

coniferous forest, regrowing clearcuts and bare soil, well distributed over the width of the scene, the Colorado cover types are not as uniformly distributed, leading to biases in the brightness gradients derived from column means. In addition, the flightline with the largest gradient was oriented 51° off the solar azimuth while the Oregon flightline was oriented 75° from the solar azimuth.

The near-simultaneous AVIRIS and Landsat 7 coverage of the area in eastern Colorado provided a unique opportunity to quantify the BRDF effects in the 30° scan angle provided by AVIRIS, normalized to Landsat that covered the area in only 0.8° scan angle. In addition BRDF effects could be measured at wavelengths beyond the $1.0 \mu\text{m}$ cutoff of airborne and spaceborne systems designed for BRDF measurements (Irons et al, 1987; Diner et al, 1999) and beyond the $1.6 \mu\text{m}$ cutoff of ground measurements (Deering et al, 1990).

Data Acquisition and Processing

On July 10, 1999, AVIRIS data were acquired in northeastern Colorado to coincide with the 11:15 MDT overflight of Landsat 7. The Landsat solar zenith angle was 26° . The AVIRIS data were acquired one hour earlier between 10:09 and 10:24 MDT at which time the average solar zenith angle was 39° . Figure 3 shows the locations and orientations of the two flight lines. The solar geometry is shown in Figure 4. Figure 5 is a representative BRDF plot for a plowed field taken from Derring (1989) onto which the AVIRIS scan directions and widths are plotted and shows that only a small portion of the response curve is covered and that the changes can be expected to be roughly linear with

scan angle. The original figure suffices for illustrative purposes even though it was plotted for a 65° solar zenith angle and 662 nm wavelength while the zenith angle in this study was approximately 40°.

AVIRIS data were atmospherically corrected to apparent surface reflectance using ATREM (Gao et al, 1993) and further corrected to the surface reflectance averaged from 100 points within a plowed field in line FM03 (fig 6) taken at 12-12:30 MDT when the solar zenith angle was 19°. This correction and normalization ensures that correction for water vapor is made on a pixel-by-pixel basis throughout the images and that errors in the model correction are removed through the normalization process. This normalization does not correct for BRDF effects associated with different overflight times, or illumination changes during the AVIRIS underflight. For comparison of Landsat 7 to AVIRIS data, Landsat 7 data were corrected for path radiance using dark object subtraction (Chavez, 1996) and corrected to reflectance using the same average spectrum of the plowed field. AVIRIS data were convolved with the bandpasses for the six Landsat 7 reflectance channels in order to be able to make a direct comparison between the sensors (fig. 7)

Results

Applying the technique outlined by Kennedy et al (1997), downtrack or column pixel averages were calculated for two, 512-line image cubes in each of the two flight lines. The results are shown in Figures 8 and 9. The variance among individual columns is too large to allow derivation of a slope corresponding to the average BRDF response. The

reason is that the landcover is not sufficiently homogeneous within an individual cube, which represents approximately 100 km² of the surface. Therefore, Landsat 7 data were utilized to correct for the brightness variations associated with different surface cover types.

Another key element to a viable comparison was accurate geometric registration. The AVIRIS data are collected with the instrument hard-mounted to the ER-2 aircraft frame. Yaw, pitch and roll attitudes measured with gyros are recorded along with GPS locations to allow accurate photogrammetric reconstruction of the pixel locations (Boardman, 1999). The Landsat data were then registered to the geo-corrected AVIRIS data. Because of the altitude of the Landsat sensor there was no perceptible BRDF effect in the image data caused by this transformation. The original AVIRIS data with 18.6 m pixels were then registered and resampled to the 30 m pixel Landsat ETM data using bilinear interpolation. A better radiometric match between the sensors was obtained using bilinear interpolation rather than cubic convolution. The bilinear resampling has little effect on the radiometry for comparison between the two sensors because of the considerably smaller AVIRIS pixels.

The AVIRIS data in the Landsat bands were ratioed to the registered Landsat data and the result multiplied by the average Landsat value for the image in the respective bands. Two AVIRIS scenes in each of the two flightlines were analyzed. Down-track averages were taken at each sample and plotted cross-track as shown in Figure 10. The plots are considerably smoother than without application of the Landsat normalization as seen in

Figures 8 and 9. A linear least-squares fit was applied to each band plot to calculate a gain and offset. Using these slopes, the multiplicative correction factors were generated, one for each sample, necessary to produce a slope of zero. These correction factors were applied to the original AVIRIS scenes convolved to TM bands to remove most of the effects of the BRDF.

Although the average BRDF is useful for making a general correction to allow comparison of the AVIRIS and Landsat images, each surface cover type can be expected to have a different BRDF. These differences can be seen in the slightly different slopes of the ratio plots for the different AVIRIS scenes. In order to quantify the differences, three surface cover types found throughout the images were chosen; 1) green crop vegetation, either corn, sorghum or sunflowers, 2) rangeland and 3) wheat stubble remaining from harvesting the previous week. At eight points across-track, a 30-sample wide swath was averaged down-track for each of the three cover classes in FM03. The AVIRIS/Landsat ratios for the cover classes along with the average BRDF from Figure 10 are shown in Figure 11. The slopes of the ratios are quite similar for each of the cover types except for green vegetation in band 1. The wavelength dependence of the BRDF will be discussed in more detail below.

A further measure of the quality of the comparison between AVIRIS and Landsat data can be seen by plotting each of the registered pixels to determine reflectance coincidence in each of the six spectral bands. The result is shown in Figure 12 for AVIRIS FM02, scene 9 without BRDF correction. FM02 exhibits less than a 5% BRDF effect across-

track as seen in Figure 10. There is significant scatter about ideal 45° line in the plot. This scatter can result from BRDF, misregistration, sensor system noise, sun angle, shadowing, and atmospheric effects associated with the time difference in the overflight between sensors. In FM02 BRDF would not be the major cause of the scatter. The slopes range from 1.121 in band 1 to 0.922 in band 7. Ideally the slopes should approach unity.

The effect of the BRDF is better demonstrated in flightline FM03 shown in the uncorrected scatterplot in Figure 13. The slopes range from 0.865 in band 1, 0.936 in band 2 to 0.833 in band 5. After BRDF correction, shown in figure 14, using the average slopes plotted in figure 11, the slopes range from 1.085 in band 1 to 0.851 in band 7.

In order to better identify the causes of the scatter about the mean slope in each of the bands, images from both flight lines with and without BRDF correction are displayed in Figures 15 and 16 along with color-coded scatter plots. Along the left side of the figures are CIR images. Along the right side are images coded to show departures from one-to-one coincidence between AVIRIS and Landsat overplotted on a band 4 image. Red indicates a higher value in Landsat than AVIRIS for the same pixel location, green the inverse and gray, perfect coincidence. In each case the lower of the two images has been corrected for an average BRDF effect shown in figure 10. In the FM02 images, the BRDF correction is very small and consequently it appears that the departures from perfect coincidence are associated with dune topography that would indicate that sun angle effects associated with the different image acquisition times are the cause. Gray in

the image implies perfect coincidence and the red and green colors appear when the reflectance value departs approximately 0.1% from the mean slope. Therefore, the images on the right in the figures show very little gray. The red and green pixel-sized spots are most likely caused by system noise, including encoding in Landsat, since the ETM+ has a lower signal-to noise ratio and reduced encoding compared to AVIRIS. Misregistration does not appear to be a significant cause of the scatter.

In line FM03 the BRDF effect is significant as shown in Figure 16. The uncorrected images in the top half of the figure show a gradient across the image, more pronounced in the right image, consistent with a relatively brighter AVIRIS image in the backscatter direction. The BRDF corrected image shows colors consistent with departures of the BRDF behavior of different surface cover types from the mean BRDF function used for correction. Again system noise appears to be a major cause of scatter.

The scatterplots in Figures 12-14 appear to demonstrate significant disagreement between the Landsat and AVIRIS reflectance values. A different representation of the data can be made with a histogram of NDVI values for Landsat AVIRIS and BRDF-corrected AVIRIS (figure 17). No significant differences are evident among Landsat and the two versions of AVIRIS even though there are visible spatial differences in the CIR images in figure 16. This implies an insensitivity in the NDVI as an index (Privette, et al, 1995, Russell et al, 1995) and the fact that the histogram representation does not display small differences.

The BRDF effects at full AVIRIS spectral resolution can be derived from the fact that two intersecting flightlines were flown, one of which was close to the sun azimuth. AVIRIS flightline FM02 was flown within 8.5° of the sun azimuth and from Figure 10 it can be seen that the BRDF effect is less than 5% across the full swath. Therefore, it should be possible to use reflectance values, invariant across the swath, to derive the BRDF effect over the full spectral range for different cover types in FM03 where the flightlines intersect. Flightlines FM02 and FM03 intersect in the southeastern corner of the area covered (fig. 3). Images of the intersecting regions are superimposed in Figure 18. Four cover types are identified by yellow shapes, each on the west and east side of the FM03 image. While the areas chosen do not contain identical cover, there is little or no BRDF effect for the sites in line FM02. As seen in Figure 11, there is a general decrease in apparent reflectance moving from west to east in FM03.

In Figure 19 we have plotted the ratios of the west/east sites for the four cover types. In FM02, the departures from unity at all wavelengths are the result of differences in spectral reflectance in the sites that are in the same class but not identical. The ratios for FM03 incorporate the intraclass differences in reflectance as well as any spectral BRDF effect. The differences in FM02 and FM03 at wavelengths short of 500 nm are dramatic.

In order to remove the intraclass spectral differences and identify spectral BRDF effects, in Figure 20, ratios of FM03/FM02, west/east ratios were plotted for each of the four classes in figure 19. At wavelengths greater than 700 nm the ratios range from approximately 1.1 to 1.15, a small 5% difference. However, short of 700 nm the ratios

rise dramatically, and in the case of Green Crops, the ratio reaches 1.6 at 450 nm. The effect is least for Wheat Stubble and greatest for Green Crops that correspond to reflectances of 11.1% and 5.9% respectively. This result is consistent with that of Sandmeier et al (1999) for ground and aircraft measurements that show that BRDF effects are inversely related to reflectance and are affected by canopy architecture and leaf area index. However, the relationship with reflectance is not consistent with the ratios observed at the bottom of the chlorophyll well at 680 nm and the green peak in vegetation at 550 nm.

The ratios in figure 20 at 550 nm are greater than at 680 nm. The logical conclusion is that increased path radiance is causing the rise in the ratios toward shorter wavelengths. Therefore, a MODTRAN 4 model was run for the conditions at the time of the AVIRIS FM03 overflight to calculate the relative scattering effects on the radiance of a 10% reflectance, lambertian scatterer over the 30° swath width. The effect is almost entirely attributable to Rayleigh scattering since the measured optical depths were very low. Figure 21 shows the results of ratioing the west/east radiance values. The atmospheric effects have the expected backscatter, however, the magnitude is much smaller than the observed BRDF effects at wavelengths short of 500 nm. The differences observed remain unexplained.

Conclusions

The comparison of AVIRIS data with Landsat data for analysis of the relative merits of each in mapping sparse vegetation cover requires attention to a variety of factors that can

cause errors. A primary consideration is registration that requires that the AVIRIS data be corrected for pitch, roll, and yaw with accurate knowledge of both position and attitude derived from 3-axis gyros placed on the instrument.

When Landsat and AVIRIS images are registered, the prime differences are attributable to BRDF effects associated with the 30° scan angle of AVIRIS and by differences in image acquisition times and sun angles. BRDF effects caused by the AVIRIS scan angle can be derived for Landsat bands by normalizing the AVIRIS data with Landsat 7 values since the AVIRIS swath width only subtends 0.8° in the Landsat data. This normalization creates a better correlation between the values from the two sensors but there are still significant differences as seen in the scatter plots. When the scatter is made visible in color difference plots, the main factor appears to be random system noise as well as differential shadowing associated with the different image acquisition times.

Another method for deriving BRDF effects for AVIRIS was demonstrated by comparing the full spectra of four different cover types in overlapping regions of two flightlines, one nearly in line with the solar azimuth and one approximately 55° to the azimuth. By choosing areas spanning the width of the latter flightline, but nearly along the flightline in the former, BRDF effects could be quantified. For each of the surface cover types, the backscatter effect was readily observed to be strongest at wavelengths short of 700 nm. Atmospheric spectral scattering effects contribute to the cause of the dramatic rise at short wavelengths in the reflectance ratio of sites from the western and eastern edges of line FM03 that had already been normalized for intraclass differences. However, the

magnitude of the backscatter effect is problematic and does not fit current models for the origin of the effect.

This study has shown that it is possible to compare airborne hyperspectral data from a sensor such as AVIRIS with Landsat. However, the aircraft data must be corrected for BRDF effects associated with a wide scan angle that covers a swath that subtends less than 1° in the Landsat scene. Landsat data can be used to normalize reflectance data in individual AVIRIS images making it possible to account for the BRDF of scenes that are heterogeneous, where column averaging to obtain the BRDF is not applicable.

Acknowledgments

The authors wish to thank Joe Boardman for providing the geometric correction files to convert our AVIRIS data to map coordinates. Bruce Kindel and Zheng Qu provided results from the MODTRAN 4 model. Greg Asner provided helpful discussions and insight concerning BRDF corrections. This research was supported by NASA GSFC contracts NAG5-6051 and NAG5-3437.

References

- Ahlbrandt, T.S., J. Swinehart and D. G. Maroney, (1983), The dynamic Holocene dune fields of the Great Plains and Rocky Mountain basins. USA in Eolian Sediments and Processes, M.E. Brookfield and T.S. Ahlbrandt Editors, Elsevier, Amsterdam.
- Boardman, J. W., (1999), Precision geocoding of low-altitude AVIRIS data: Lessons learned in 1998, *Summaries of the Eighth JPL Airborne Earth Science Workshop, JPL Publication 99-17*, 63-68.
- Buckley, R., (1987), The effect of sparse vegetation on the transport of dune sand by wind, *Nature*, 325: 426-428.

- Chavez, P.S., (1996), Image-based atmospheric corrections – revisited and improved, *Photogrammetric Engineering & Remote Sensing* 62: 1025-1036.
- Diner, D. J., Asner, G. P., Davies, R., Knyazikhin, Y., Muller, J.-P., Nolin, A. W., Pinty, B., Schaaf, C. B. and Stroeve, J., (1999), New directions in Earth observing: Scientific applications of multiangle remote sensing, *Bull. Am. Met. Soc.* 80: 2209-2228.
- Deering, D. W., (1989), Field measurements of bidirectional reflectance, in Theory and Applications of Optical Remote Sensing, G. Asrar, ed., Wiley & Sons, New York, 734 pp.
- Deering D.W., Eck, T.F. and Otterman, J., (1990), Bidirectional reflectances of selected desert surfaces and their 3-parameter soil characterization, *Agricultural and Forest Meteorology*, 52: 71-93
- Deering, D.W., Middelton, E.M., Irons, J.R., Blad, B.L., Waltershea, E.A., Hays, C.J., Walthall, C., Eck, T.F., Ahmad, S.P. and Banerjee, B.P., (1991), Prairie grassland and bi-directional reflectances measured by different instruments at the FIFE site, *J. Geoph. Res.-Atm.* 97: 18887-18903
- Forman, S.L., Goetz, A.F.H, and Yuhas, R.H., (1992), Large scale stabilized dunes on the High Plains of Colorado: Understanding the landscape response to Holocene climates with the aid of images from space, *Geol.* 20: 145-148
- Gao, B.-C., Heidebrecht, K.B., and Goetz, A.F.H., (1993), Derivation of scaled surface reflectances from AVIRIS data, *Remote Sens. Environ.* 44: 165-178
- Green, R.O., Eastwood, M.L., Sartare, C.M., Chrien, T.G., Aronsson, M., Chippendale, B.J., Faust, J.A., Pavri, B.E., Chovit, C.J., Solis, M.S., Olah, M.R., and Williams, O., (1998), Imaging spectroscopy and the Airborne Visible Infrared Imaging Spectrometer (AVIRIS). *Remote Sens. Environ.* 65: 227-248.
- Irons, J. R. and Labovitz, M.L., (1982), A data analytic approach to look-angle radiance adjustment, *J. Applied Photographic Eng.* 8: 128-137.
- Irons, J.R., Johnson, B.L., and Linebaugh, G.H., (1987), Multiple-angle observations of reflectance anisotropy from an airborne linear-array sensor. *IEEE Trans. Geosci. Remote Sens.* 25: 372-383.
- Irons, J.R., Ranson, K.J., Williams, D.L., Irish, R.R., and Huegel, F.G., (1991), An off-nadir-pointing imaging spectrometer for terrestrial ecosystem studies. *IEEE Trans. Geosci. Remote Sens.* 29: 66-74.

- Irons, J.R., Campbell, G.S., Norman, J.M., Graham, D.W., and Kovalick, W.M., (1992), Prediction and measurement of soil bidirectional reflectance. *IEEE Trans. Geosci. Remote Sens.* 30: 249-260.
- Jorgenson, D. W., (1992), Use of soils to differentiate dune age and to document spatial variation in eolian activity, Northeastern Colorado, USA, *Jour. Of Arid Environ.* 23: 19-36.
- Kennedy, R.E., Cohen, W.B., and Takao G., (1997), Empirical methods to compensate for a view-angle-dependent brightness gradient in AVIRIS imagery. *Remote Sens. Environ.* 62: 277-291.
- Kimes, D. S. (1983), Dynamics of directional reflectance factor distributions for vegetation canopies. *Appl. Opt.* 22: 1364-1372.
- Middelton, E.M., Deering, D.W., and Ahmad, S.P., (1987), Surface Anisotropy and hemispheric reflectance for a semiarid ecosystem. *Remote Sens. Environ.* 23: 193-212.
- Muhs, D.R., Stafford, T.W., Cowherd, S.D, Mahan, S.A., Kihl, R., Maat, P.B., Bush, C.A. and Nehring, J., (1996), Origin of the late Quaternary dune fields of northeastern Colorado. *Geomorph.* 17: 129-149.
- Muhs, D.R., (1998), Activation of Great Plains dune sand during the 1930's drought, Geological Soc. Of Am. Annual Meeting Abstracts.
- Privette, J. L., Myneni, R. B., Emery, W. J. and Pinty, B., (1995), Inversion of a soil bidirectional reflectance model for use with vegetation reflectance models, *Jour. Geoph. Res-Atmospheres*, 100: 25497-25508.
- Russell, C.A., Walthall, C.L., Irons, J.R., and deColstoun, E.C.B., (1995), Comparison of airborne and surface spectral bidirectional reflectance factors, spectral hemispherical reflectance and spectral vegetation indices. *J. Geophys. Res. Atmos.* 100: 25509-25522.
- Sandmeier, S.R., Middleton, E.M., Deering, D.W., and Qin, W.H., (1999), The potential of hyperspectral bidirectional reflectance distribution function data for grass canopy characterization. *J. Geophys. Res. Atmos.* 104: 9547-9560.
- Woodhouse C. A. and Overpeck, J. T., (1998), 2000 years of drought variability in the central United States, *Bull. Am. Met. Soc.* 79: 2693-2714.
- Wunder, J.R., Kaye, F.W., and Carstensen, V., (1999), Americans View Their Dust Bowl Experience, University of Colorado Press, Niwot, CO, 429.

Figure Captions

- Figure 1. Landsat 5 TM CIR image of the Fort Morgan dune field in northeastern Colorado showing destabilized soils in a pivot-irrigated field.
- Figure 2. The High Plains consists of approximately 800,000 sq. km extending from South Dakota to Texas. The 100,000 sq. km of Holocene sandy soils are shown in gray and extend through 32 Landsat scenes in the study region.
- Figure 3. Location map for the AVIRIS underflights. Images are from the 15 m pan band 8 of the Landsat 7 ETM+. The left inset shows the Roggen, CO vegetation cover test site and a view from the ground. The right inset shows the ground spectral reflectance test site, a plowed field, near Brush, CO.
- Figure 4. AVIRIS underflight tracks in northeastern Colorado. Track FM02, is aligned within 8.5° degrees of the solar azimuth. Track FM03 is aligned 51.1° clockwise from the solar azimuth.
- Figure 5. A typical BRDF plot for a plowed field showing the two AVIRIS flightlines and their relationships to the full BRDF response. The BRDF effects discussed in this paper are relatively minor. After Deering (1989)
- Figure 6. ATREM-corrected AVIRIS data for a plowed field near Brush, Colorado. The field spectrum is an average of 100 spectra taken between 12 and 12:30 PM MDT on the day of the overflight over a 50 x 100 m segment of a plowed field.
- Figure 7. Landsat bandpasses and their center positions on AVIRIS spectra of soil (top) and green vegetation (bottom).
- Figure 8. Column sums for two AVIRIS scenes in flightline FM02 in each of the Landsat bands. The scenes are too heterogeneous to provide information about average brightness variations associated with BRDF effects across the scene.
- Figure 9. Same as figure 8 for flightline FM03.
- Figure 10. Flightlines shown in figures 8, 9 that have been corrected for reflectance variations using coregistered Landsat 7 data.
- Figure 11. BRDF responses in FM03 obtained by classifying the images into 3 classes and averaging the Landsat corrected average brightness in 8-30 pixel wide columns. The solid circles show the average of all pixels in the 30 pixel wide columns.
- Figure 12. Scatterplots of Landsat vs. AVIRIS pixel values in each of the Landsat 7 bands in flightline FM02.

Figure 13. Scatterplot of Landsat vs. AVIRIS pixel values in each of the Landsat 7 bands in flightline FM03.

Figure 14. Same as figure 13, but corrected for BRDF from figure 11.

Figure 15. a) CIR of an AVIRIS scene in FM02; b) Band 4 plot of Landsat vs. AVIRIS identical to figure 12 with all Landsat values higher than AVIRIS values plotted in red and those less in green; c) The colors in b plotted over a band 4 b&w image. The reflectance difference at the red-green boundary is 0.1%. d) BRDF corrected CIR from a; e) BRDF-corrected version of b; f) BRDF-corrected version of c.

Figure 16. a) CIR of an AVIRIS scene in FM03; b) Band 4 plot of Landsat vs. AVIRIS identical to figure 12 with all Landsat values higher than AVIRIS values plotted in red and those less in green; c) The colors in b plotted over a band 4 b&w image. The reflectance difference at the red-green boundary is 0.1%. d) BRDF corrected CIR from a; e) BRDF-corrected version of b; f) BRDF-corrected version of c.

Figure 17. Histogram of NDVI for the entire AVIRIS FM03 flightline as calculated from Landsat data covering the same area, from AVIRIS and the BRDF-corrected AVIRIS.

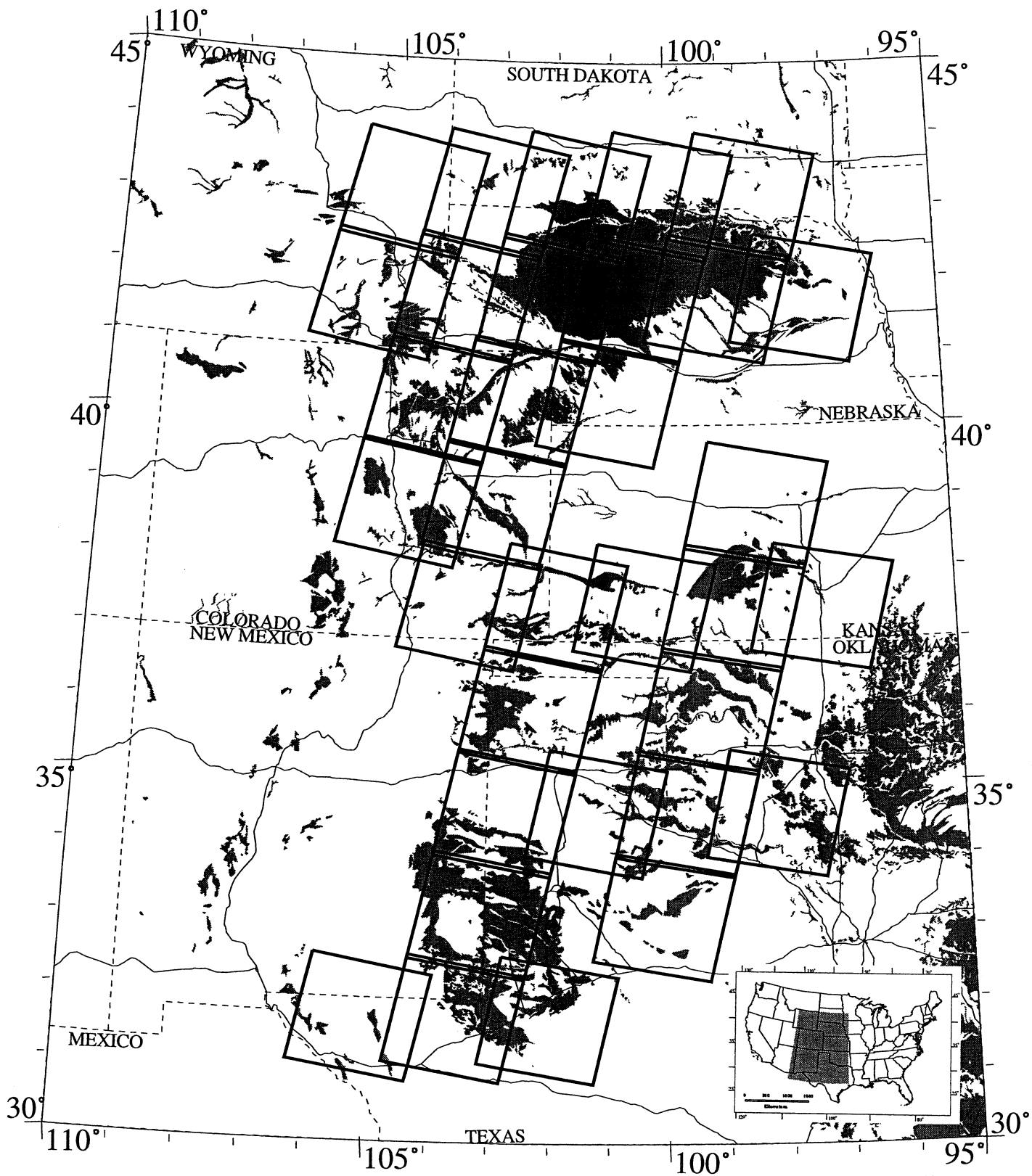
Figure 18. AVIRIS CIR images of the area of intersection of flightlines FM02 and FM03. The numbered areas correspond to four different cover types chosen to span the FM03 flightline and, therefore, exhibit the greatest BRDF effects. 1) Rangeland; 2) Wheat Stubble; 3) Conservation Reserve Program (CRP) land; 4) Irrigated Green Crops.

Figure 19. Ratios of AVIRIS spectra from both FM02 and FM03, taken West/East, for each of the 4 different cover types identified in Figure 18. The strongest BRDF or atmospheric effects are evident at the shortest wavelengths.

Figure 20. Ratios of the ratio spectra from Figure 19, FM03/FM02 for the 4 different cover types. The ratios remove the effect of intraclass differences in the cover types.

Figure 21. Ratio of the radiances of a hypothetical 10% reflectance lambertian surface situated on the west and east edges of the FM03 flightline calculated using MODTRAN4 at 15 cm^{-1} resolution.





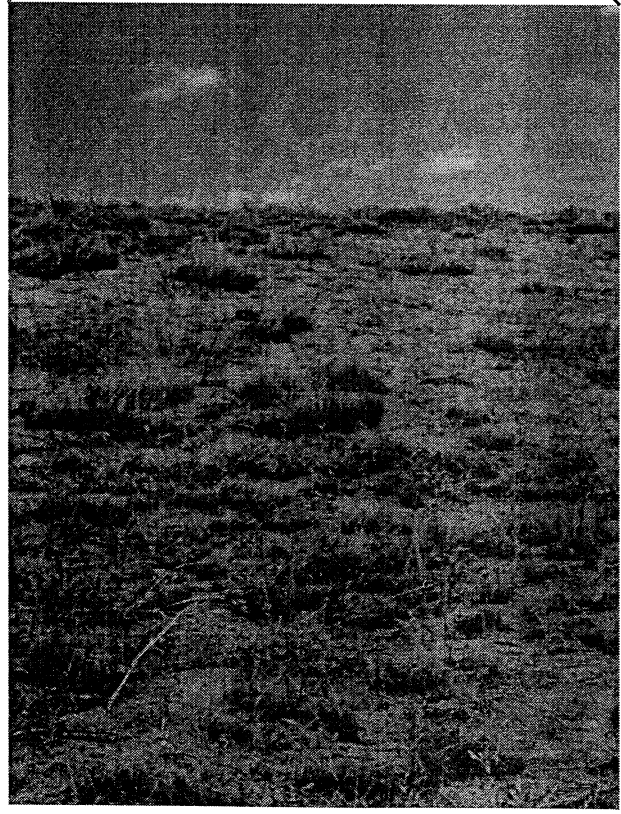
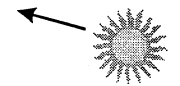
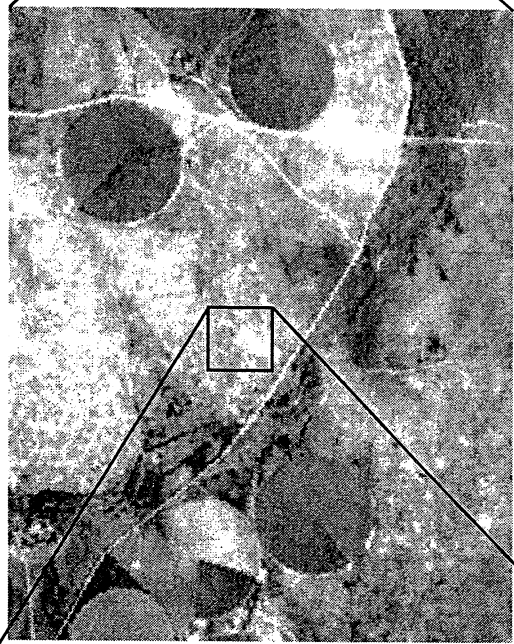
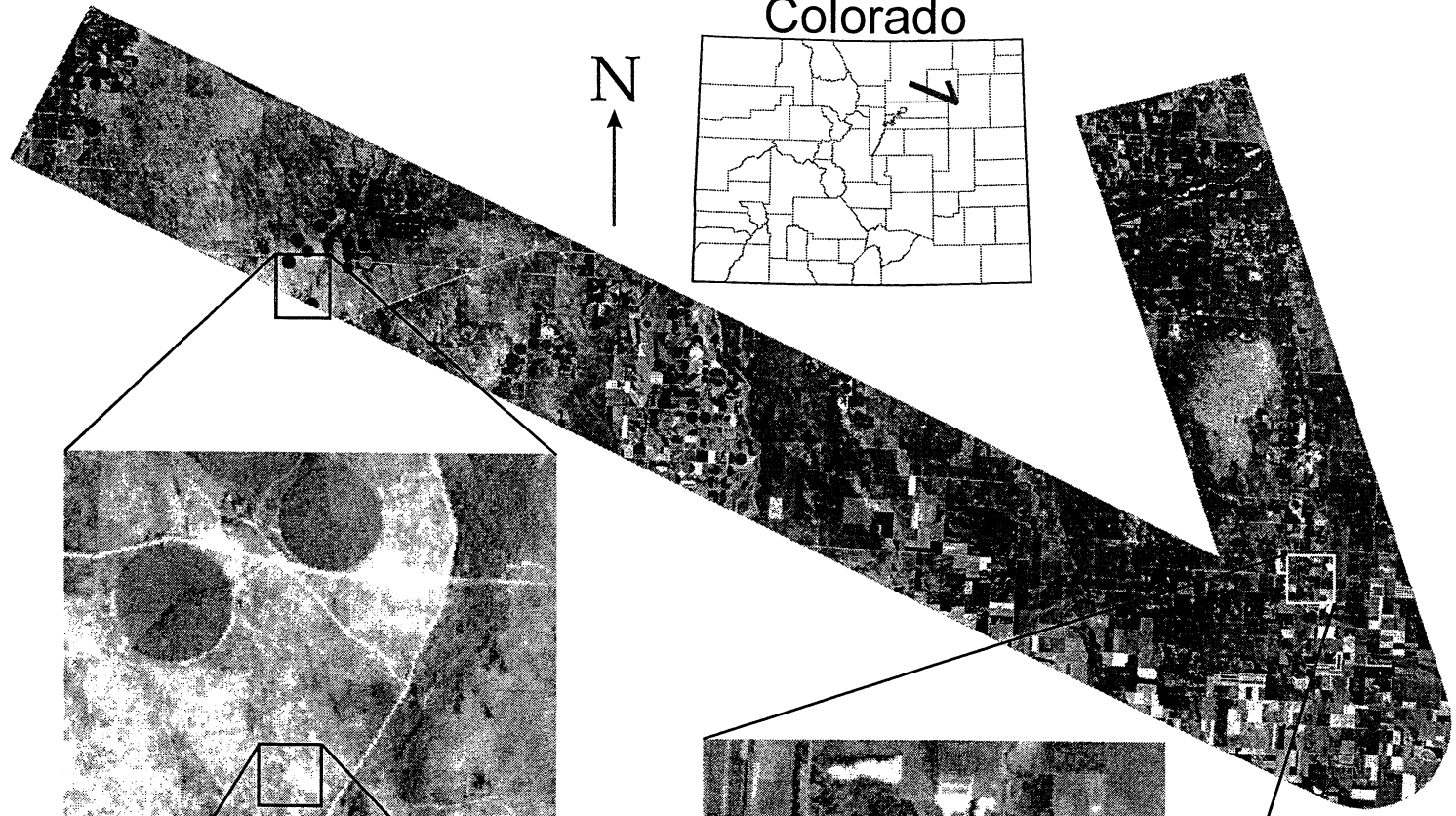
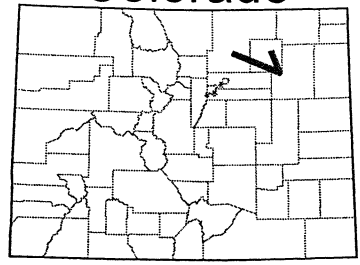
■ Sandy soils

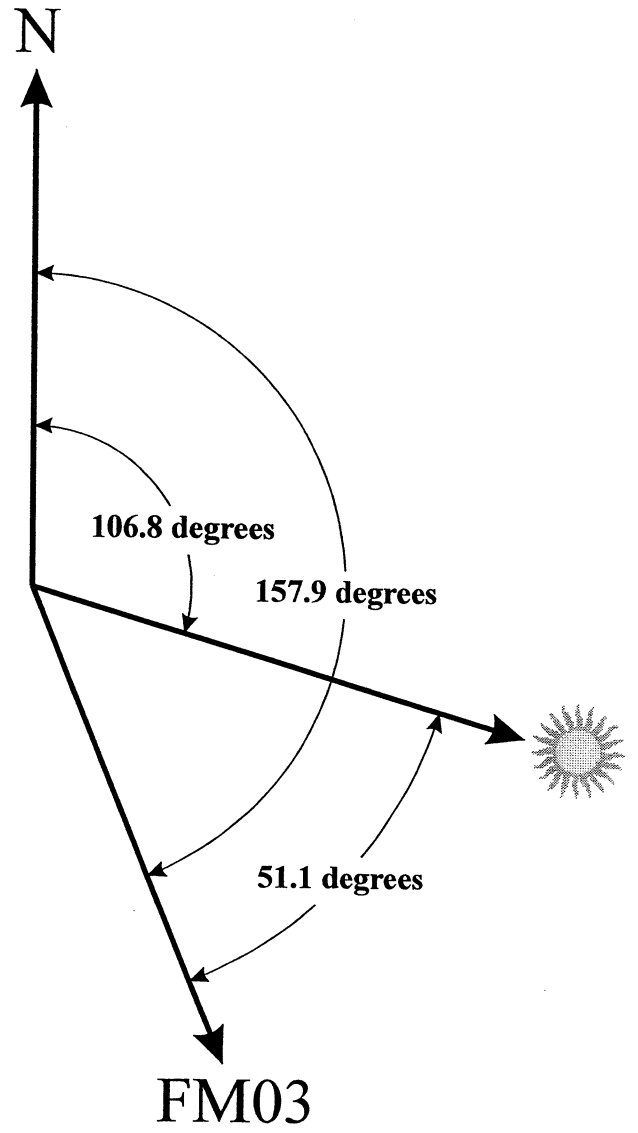
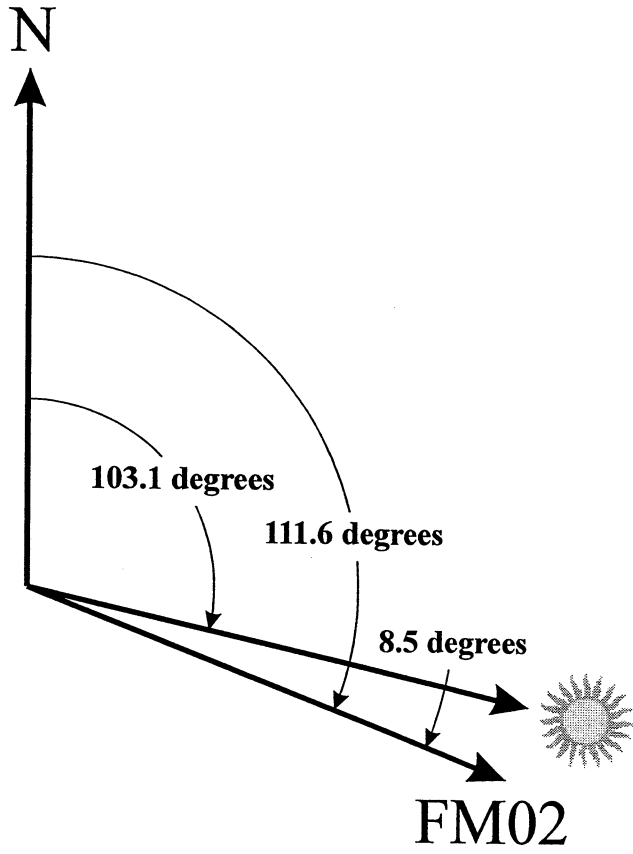
0 100 200 300 400 500

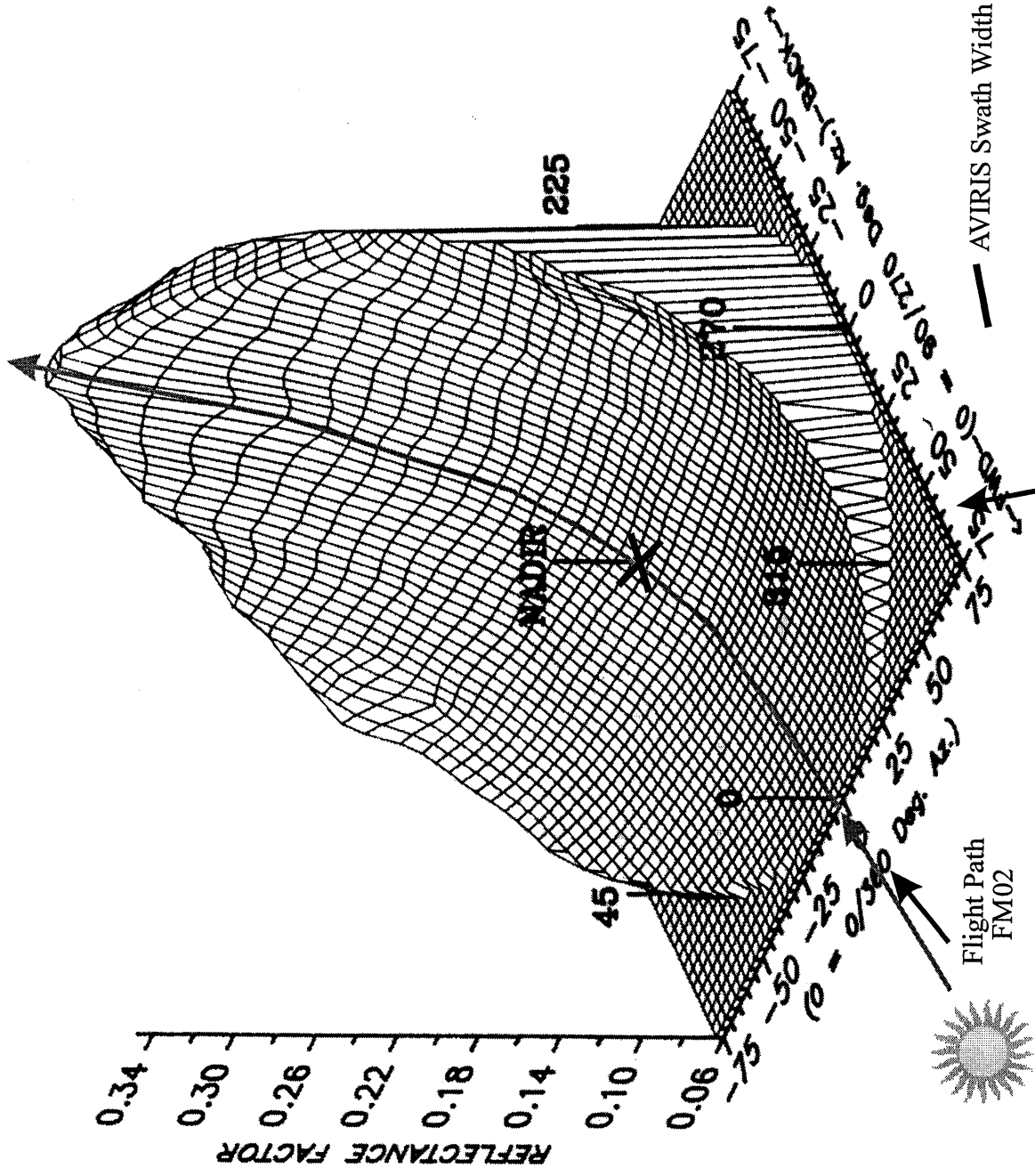
KILOMETERS



Colorado

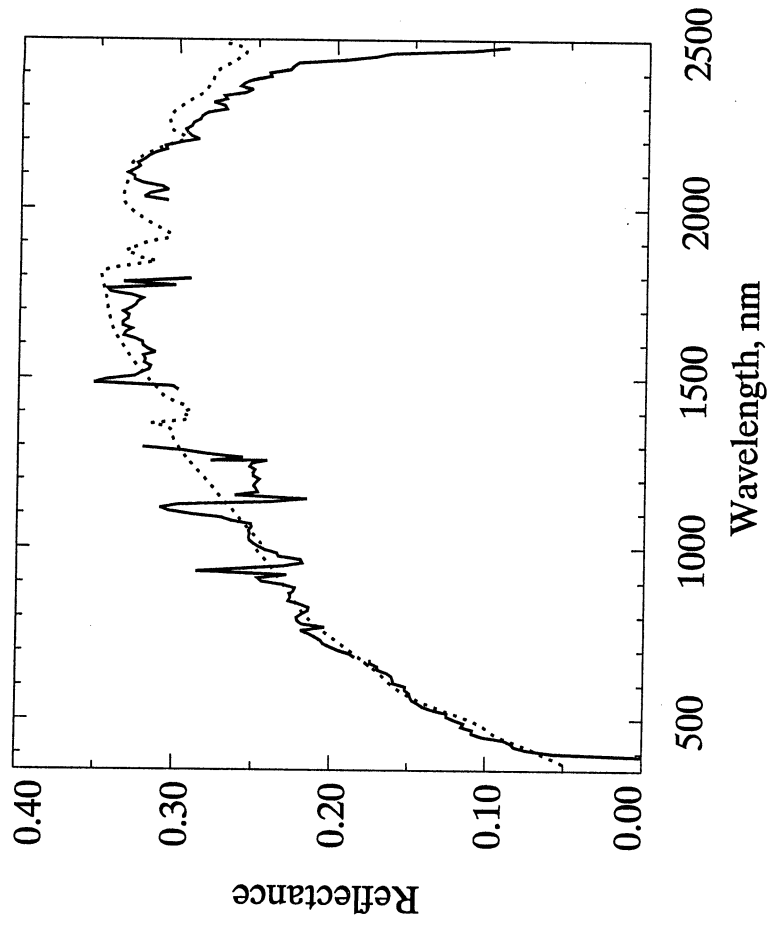


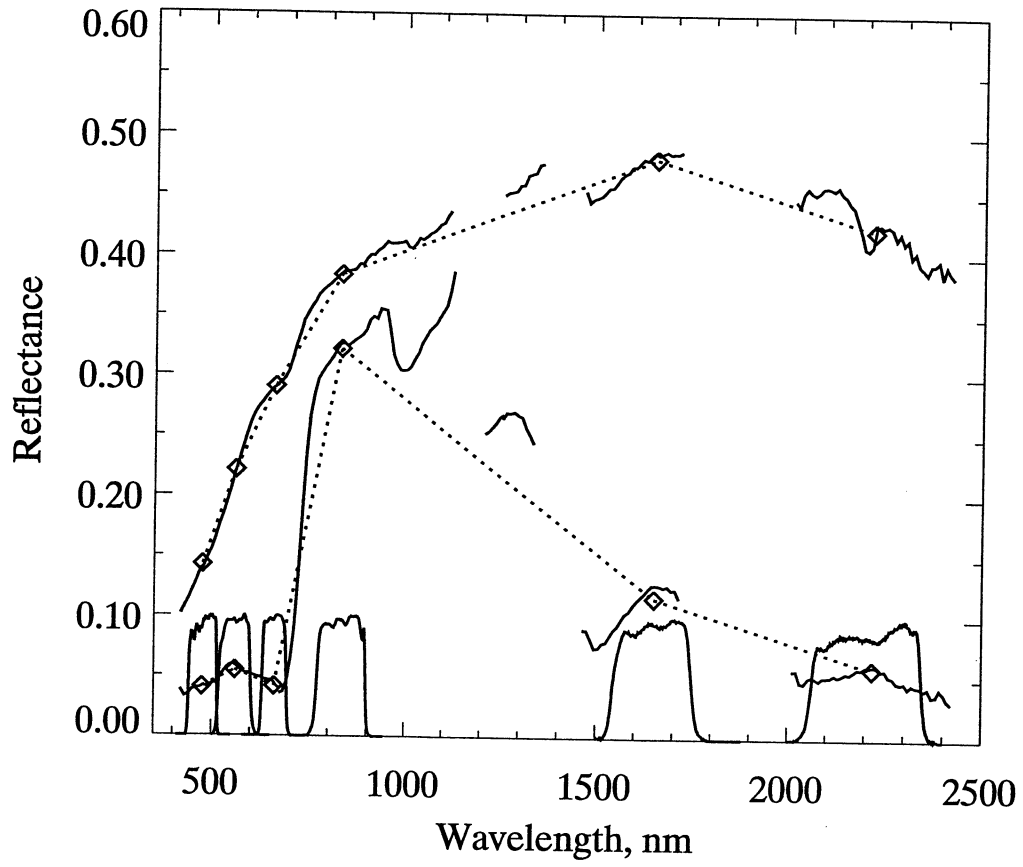




Flight Path FM03

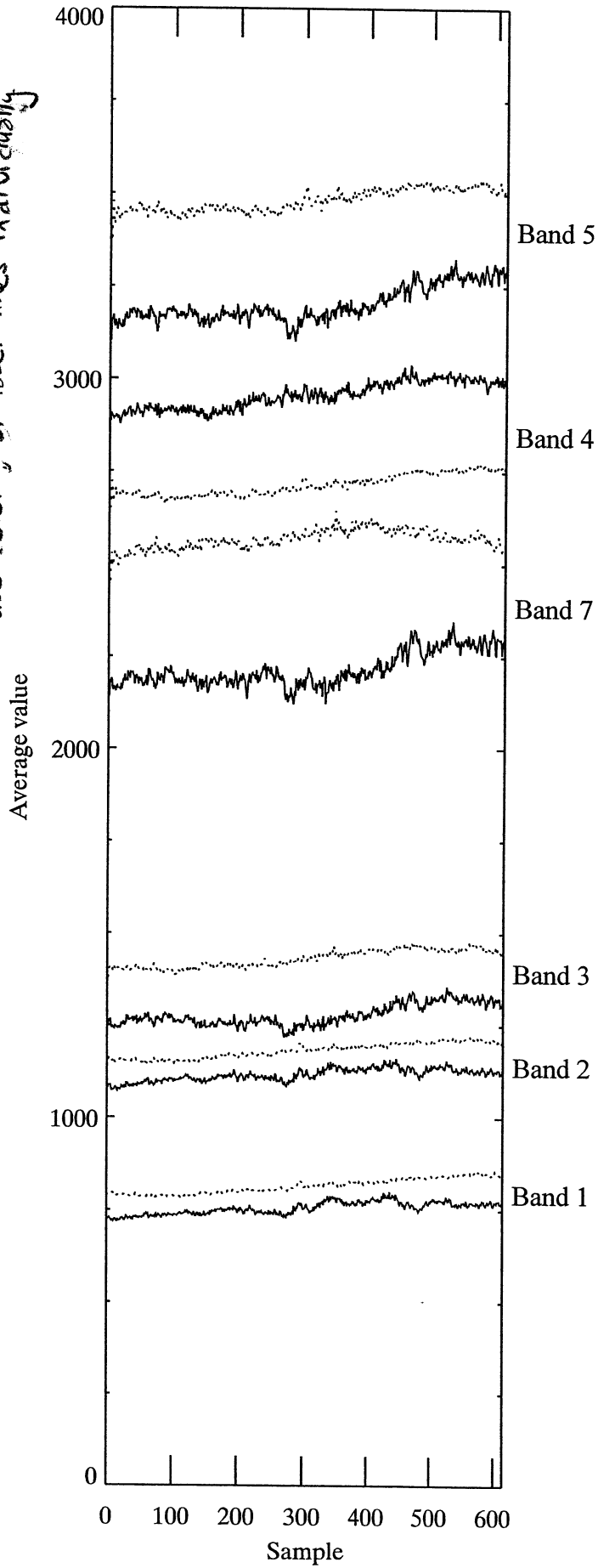
Flight Path FM02



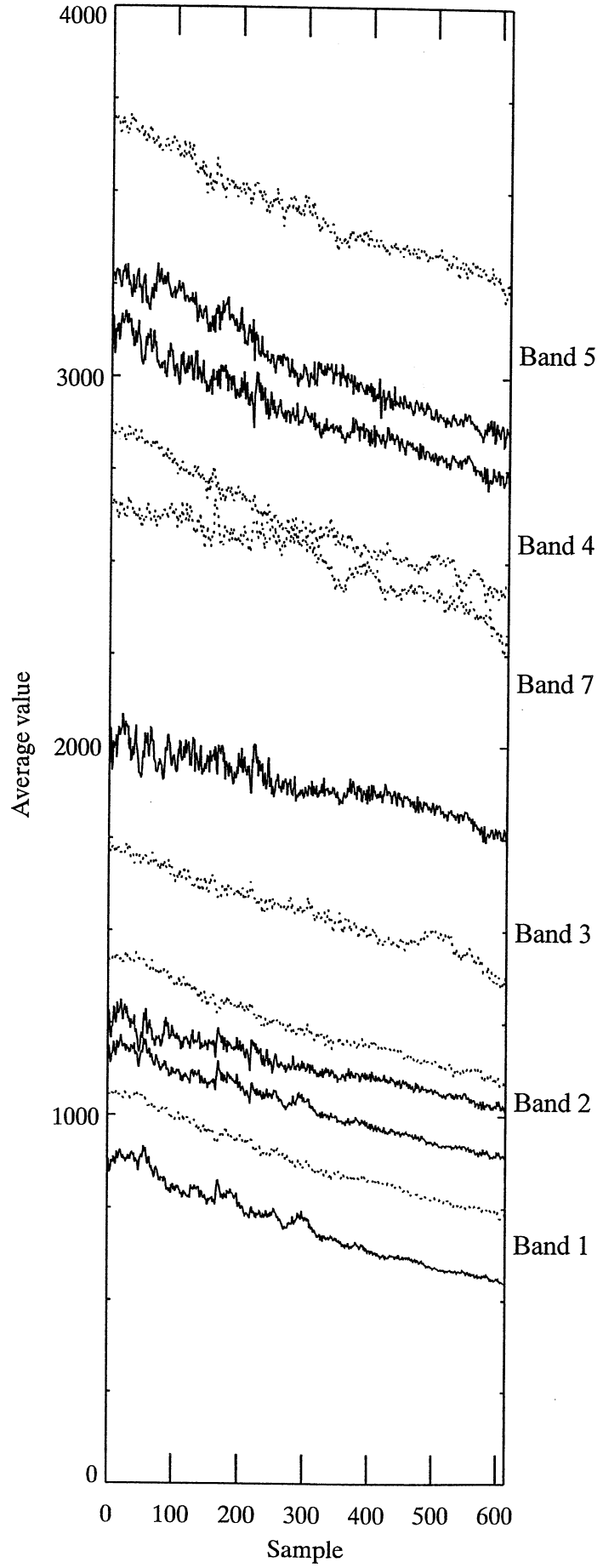


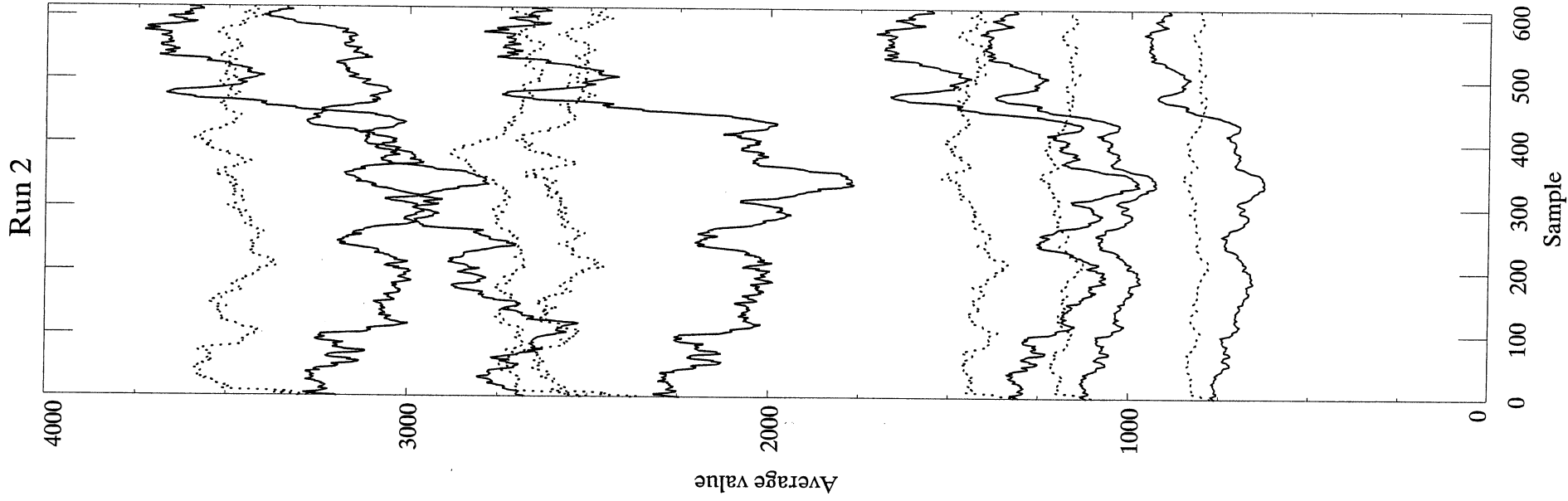
it's impossible to tell which bands match which lines
use color or label lines individually

Run 2



Run 3





Band 5

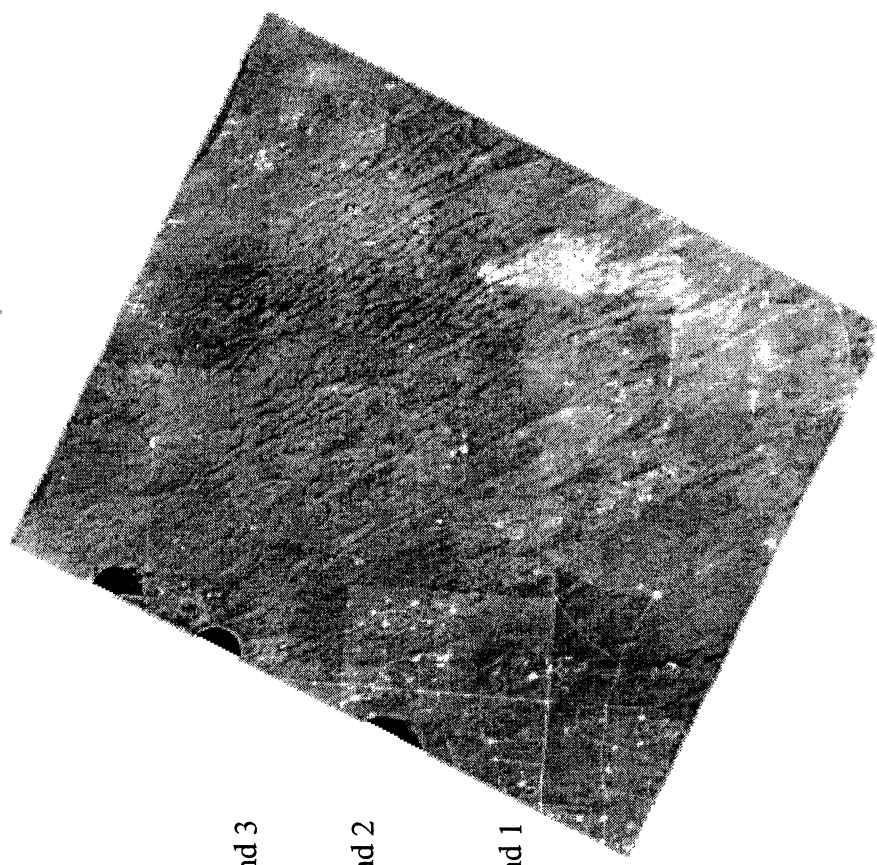
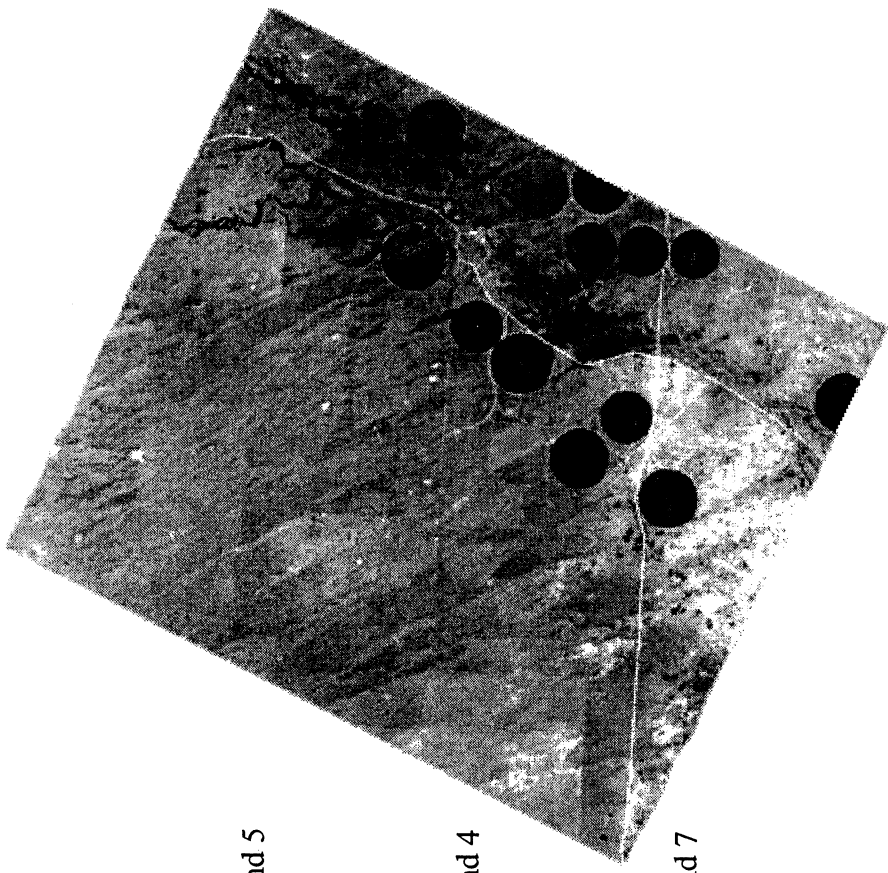
Band 4

Band 7

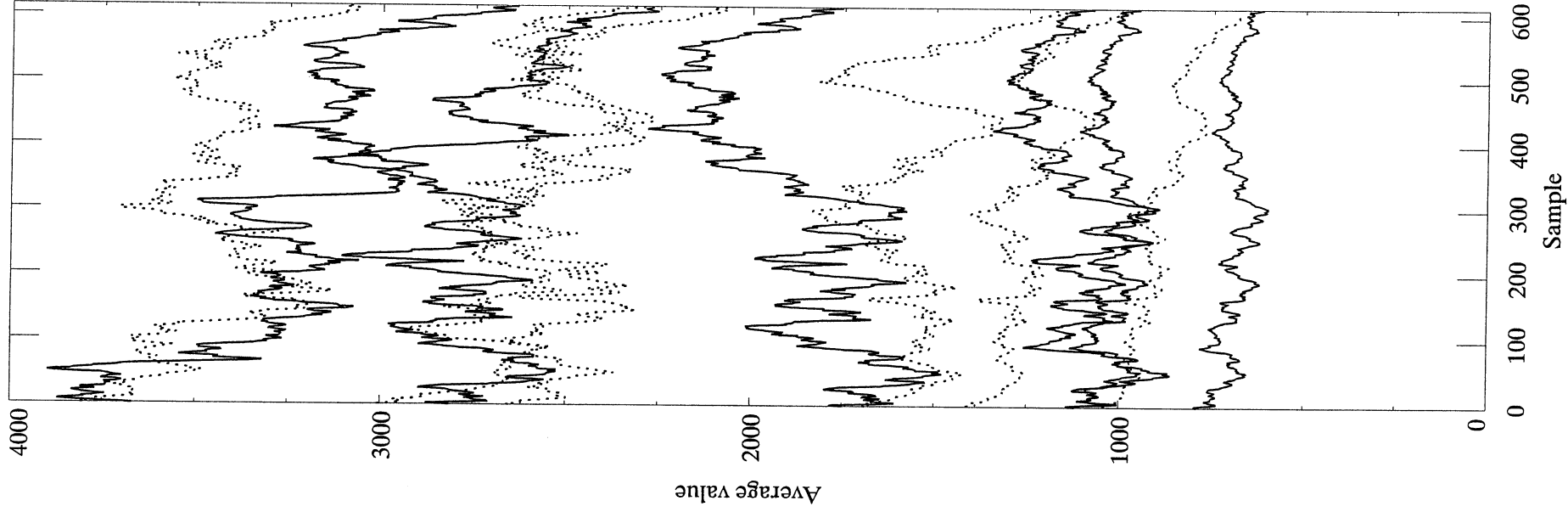
Band 3

Band 2

Band 1



Run 3



Band 5

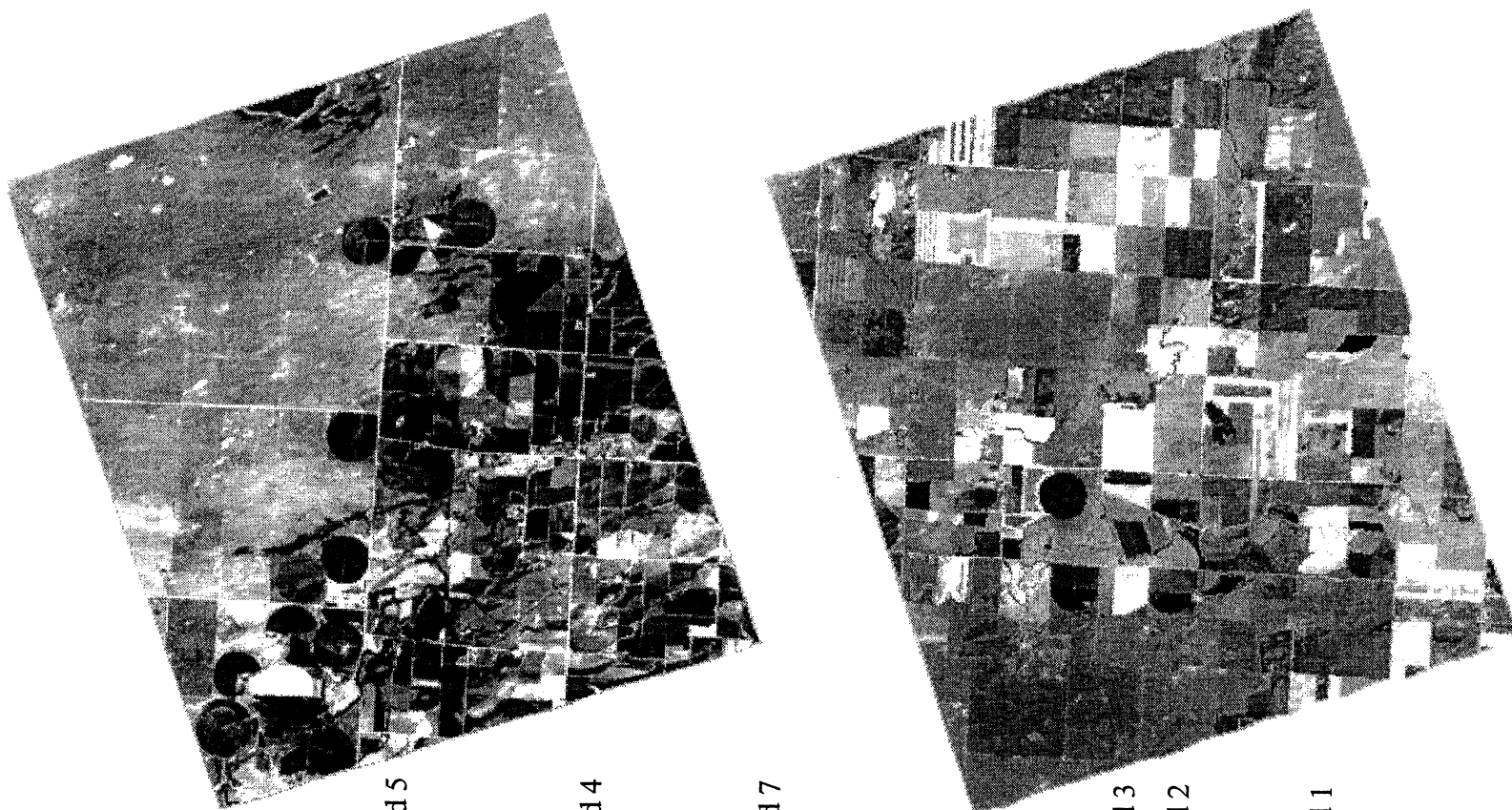
Band 4

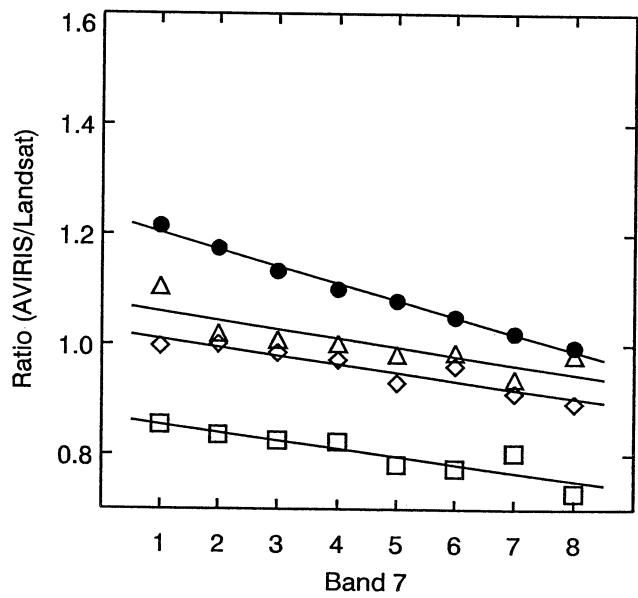
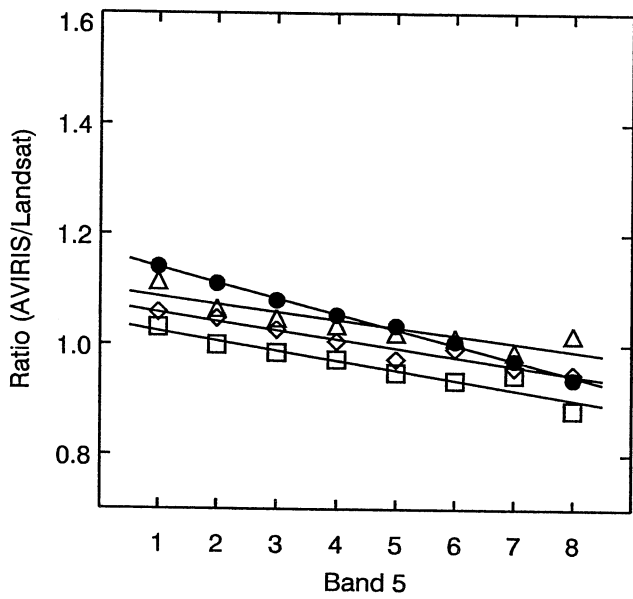
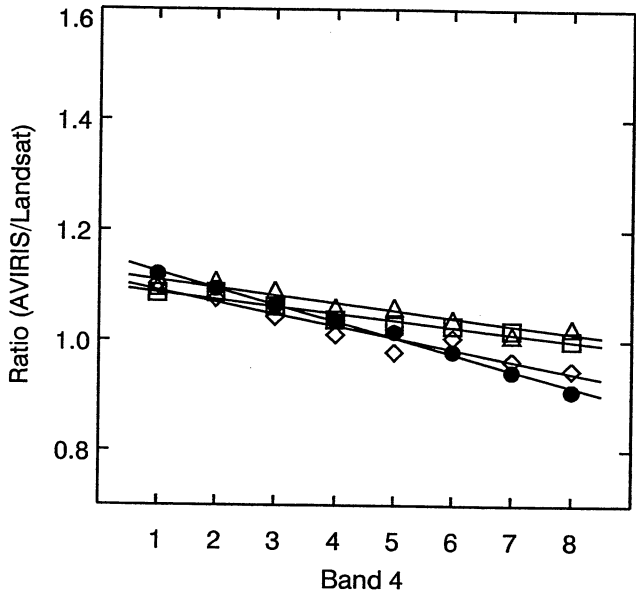
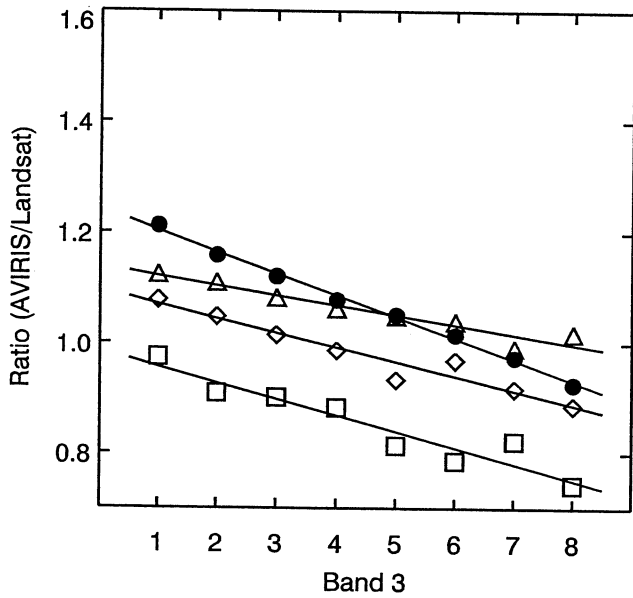
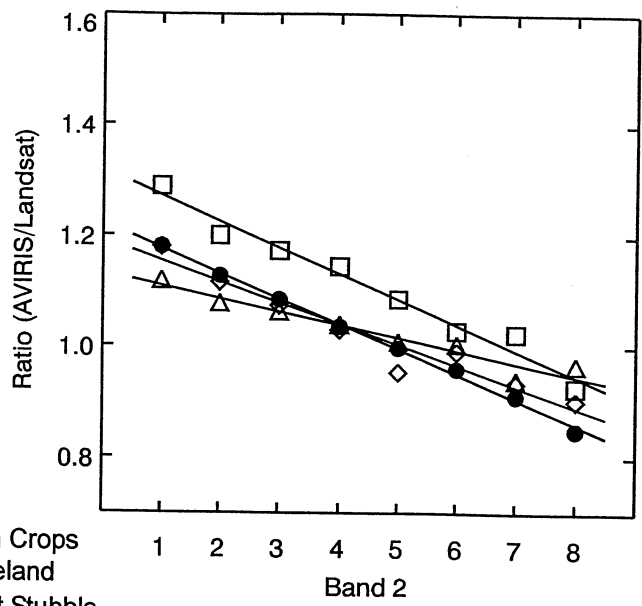
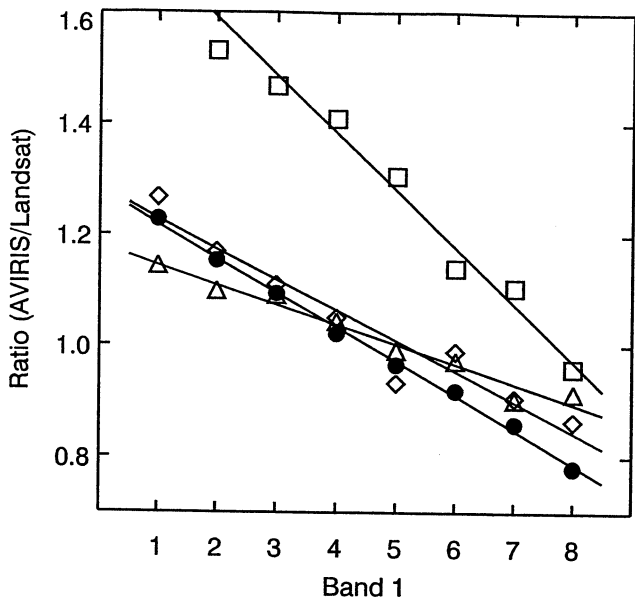
Band 7

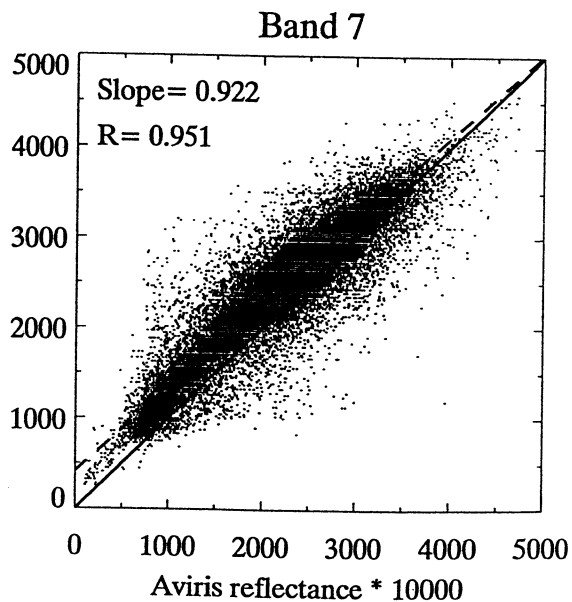
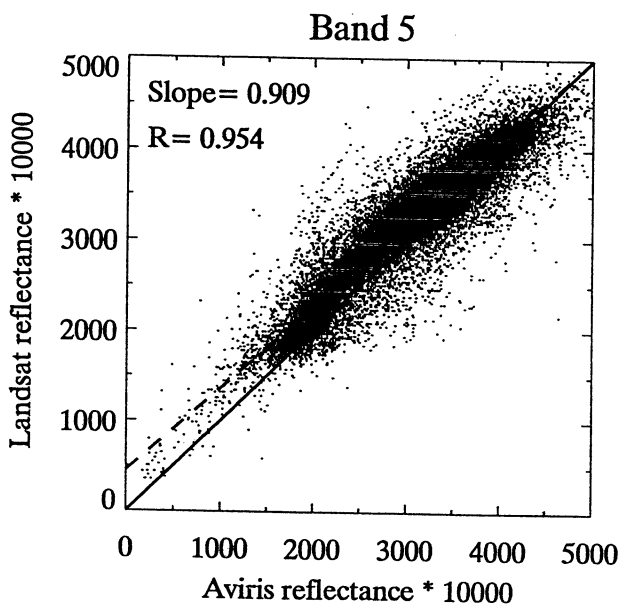
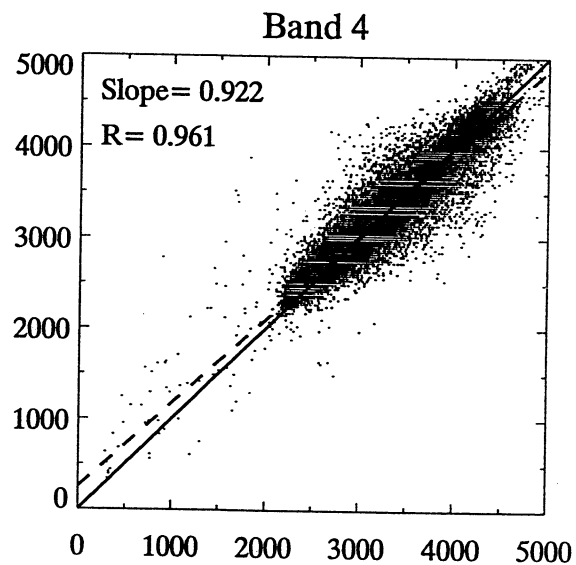
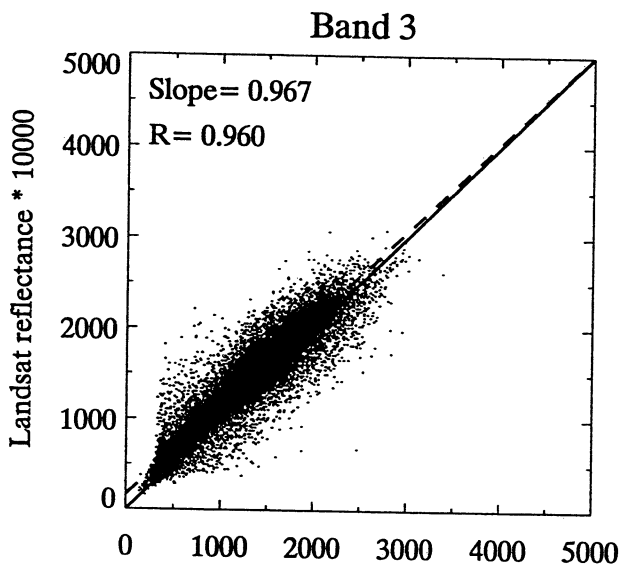
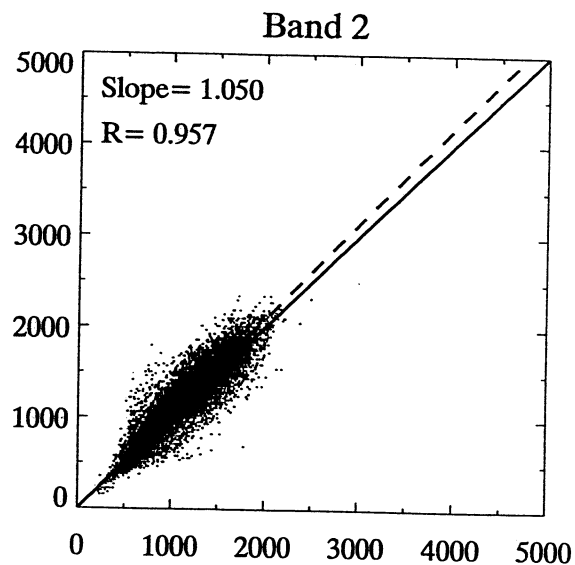
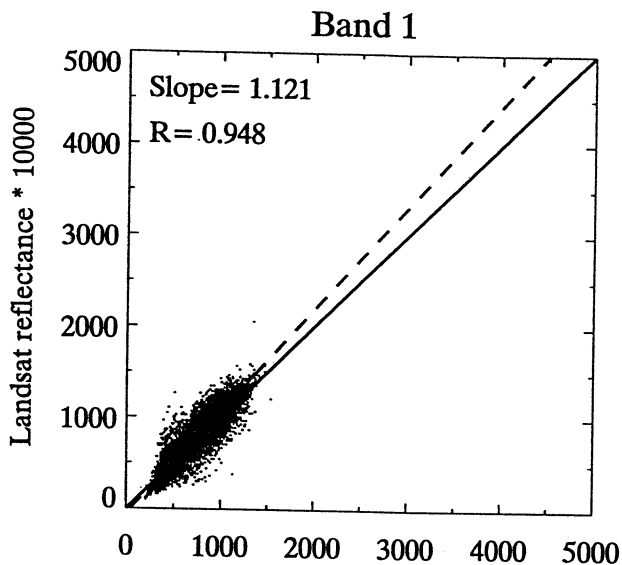
Band 3

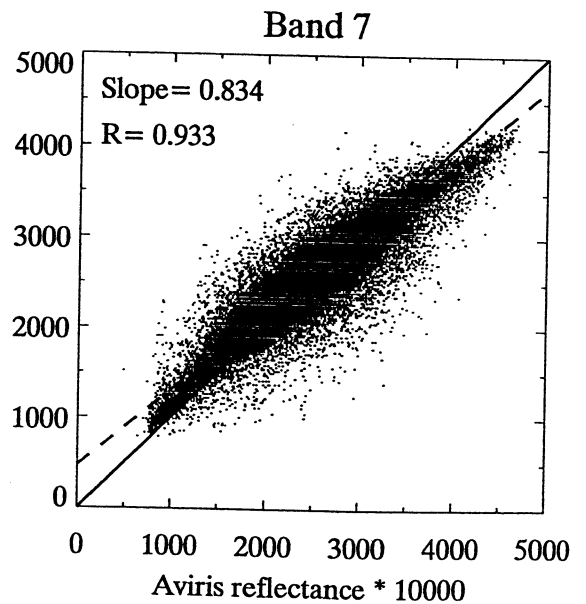
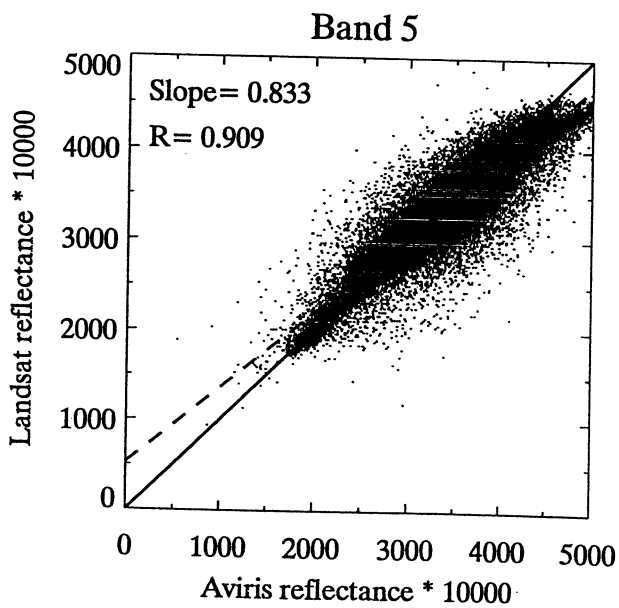
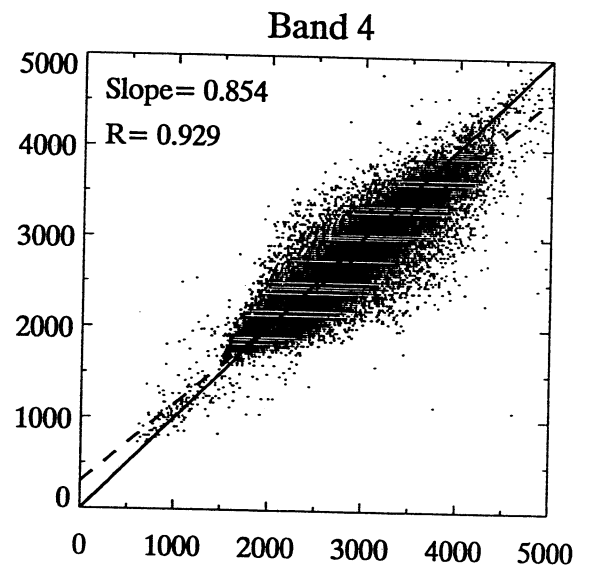
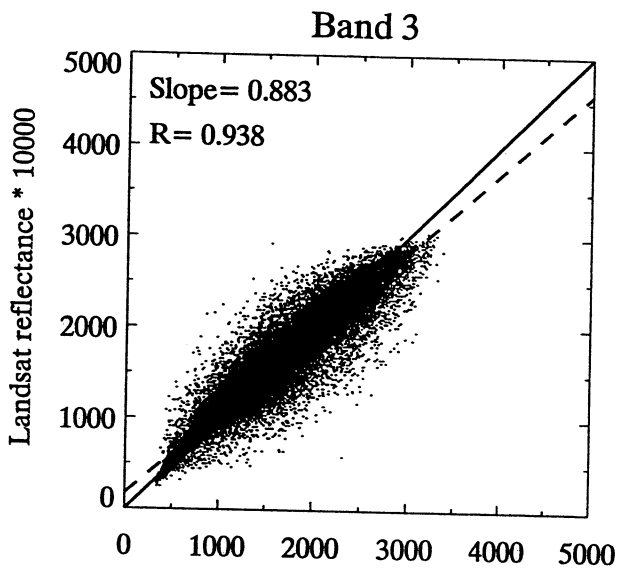
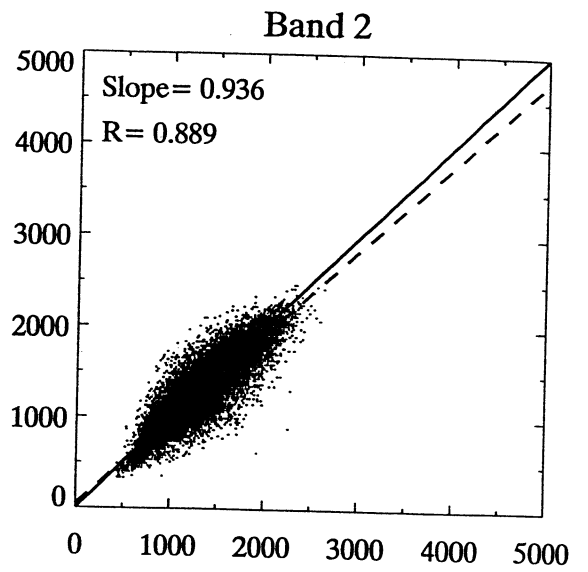
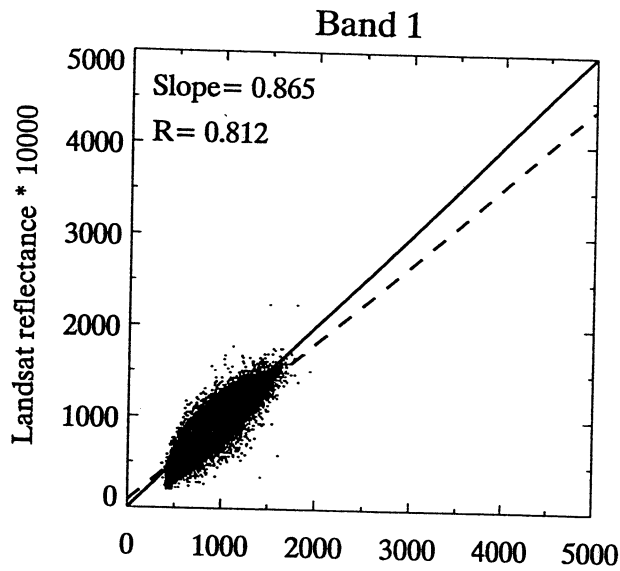
Band 2

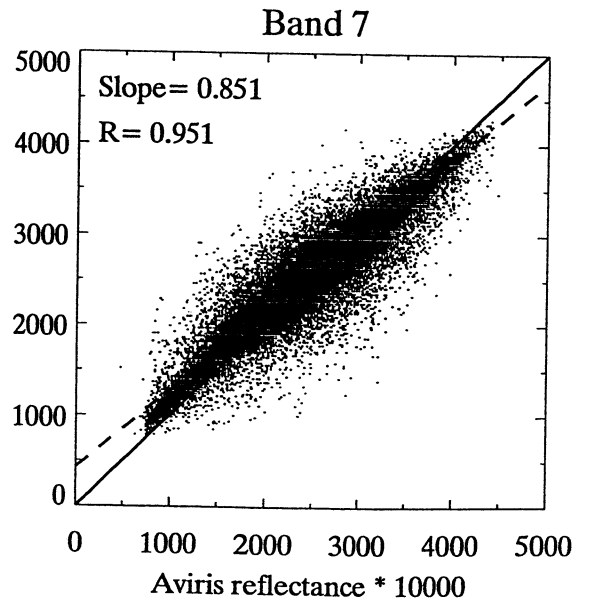
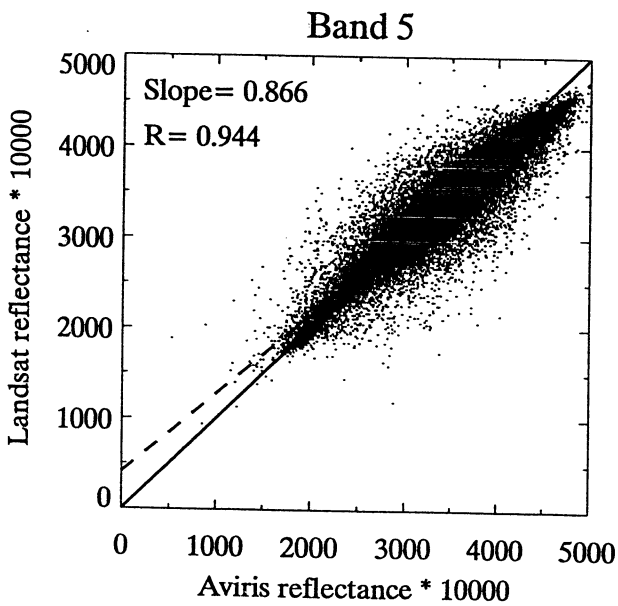
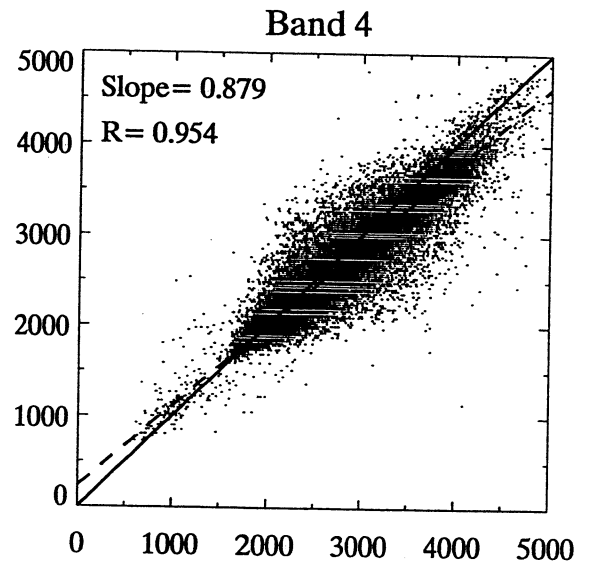
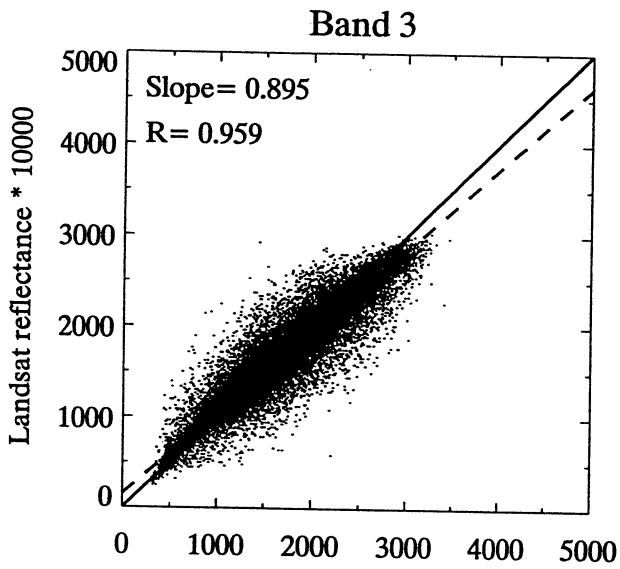
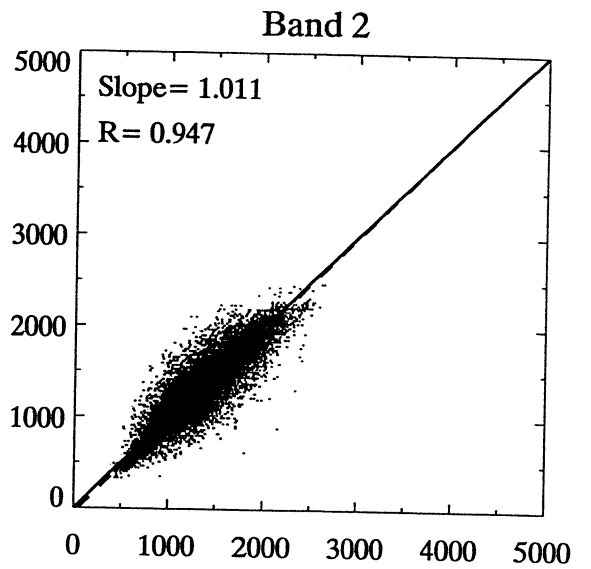
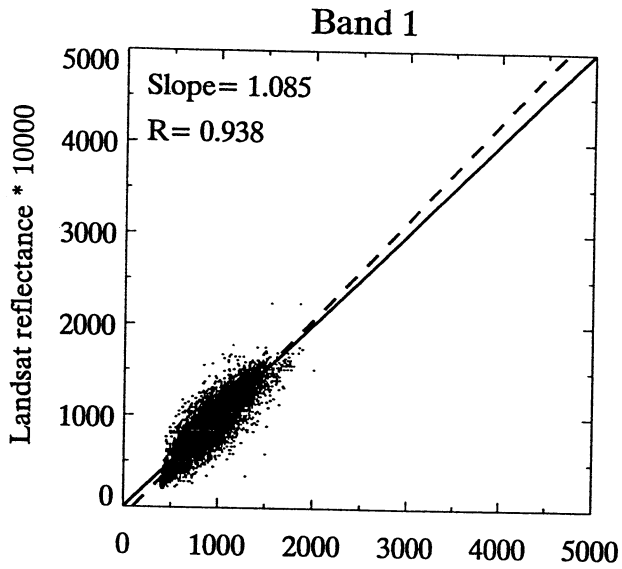
Band 1

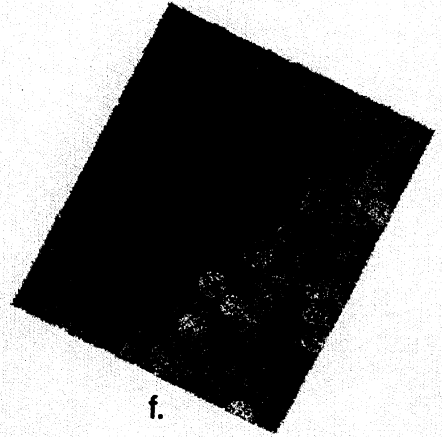
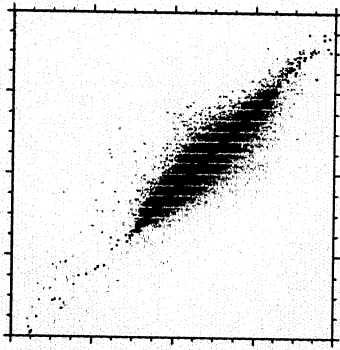
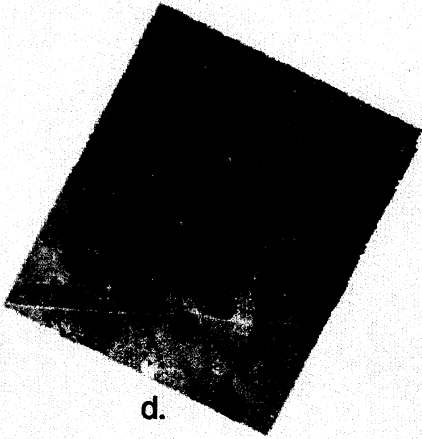
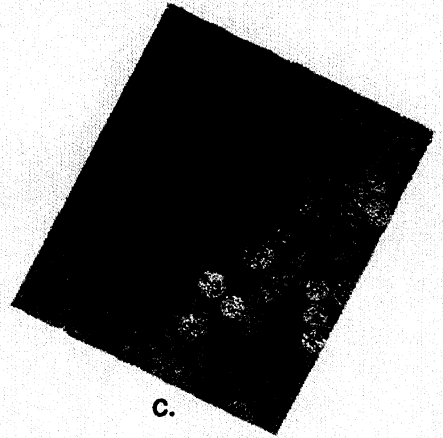
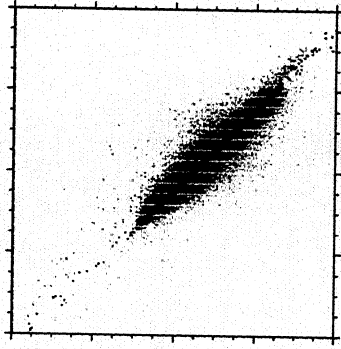
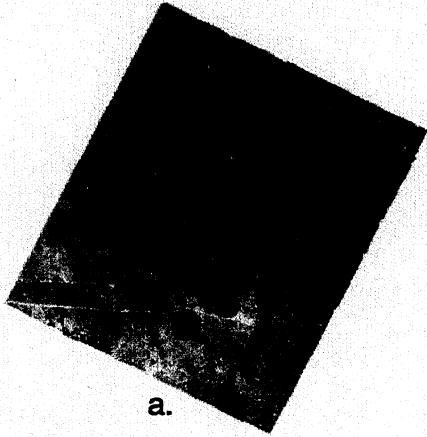


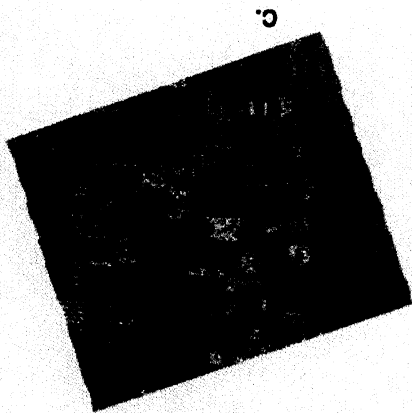
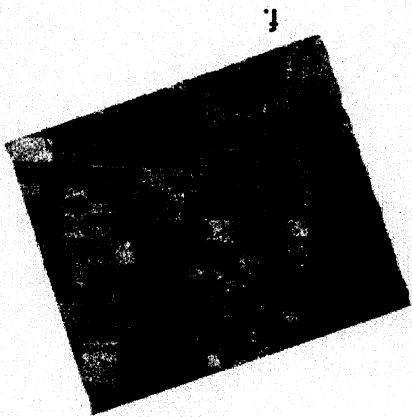
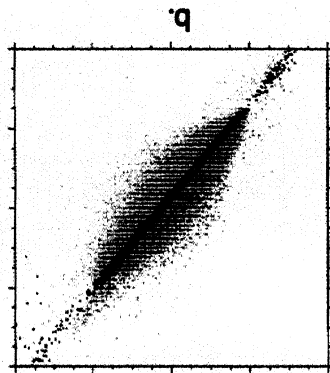
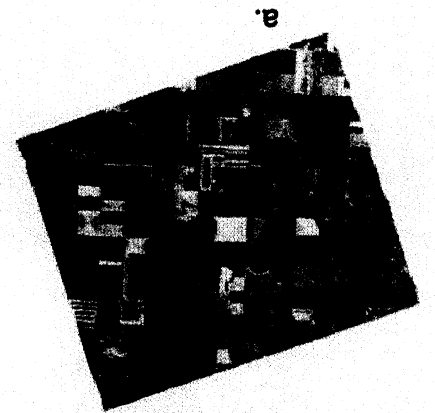
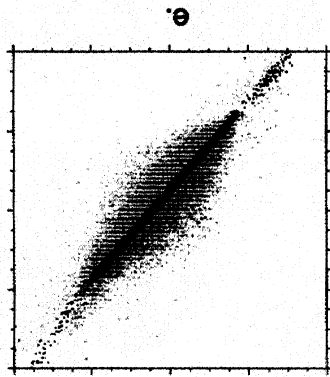
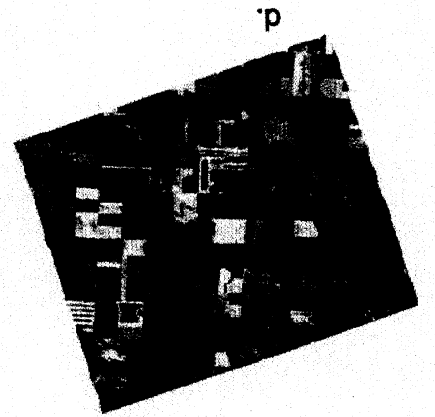


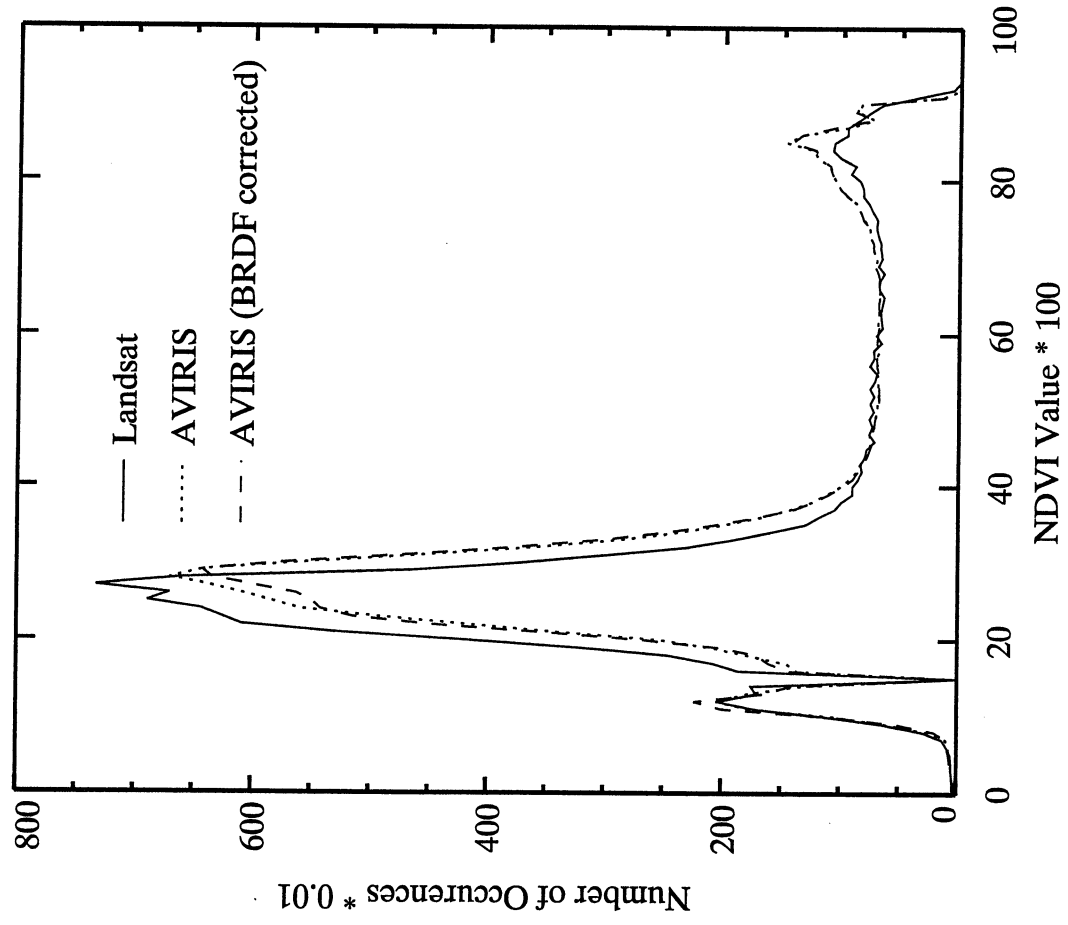






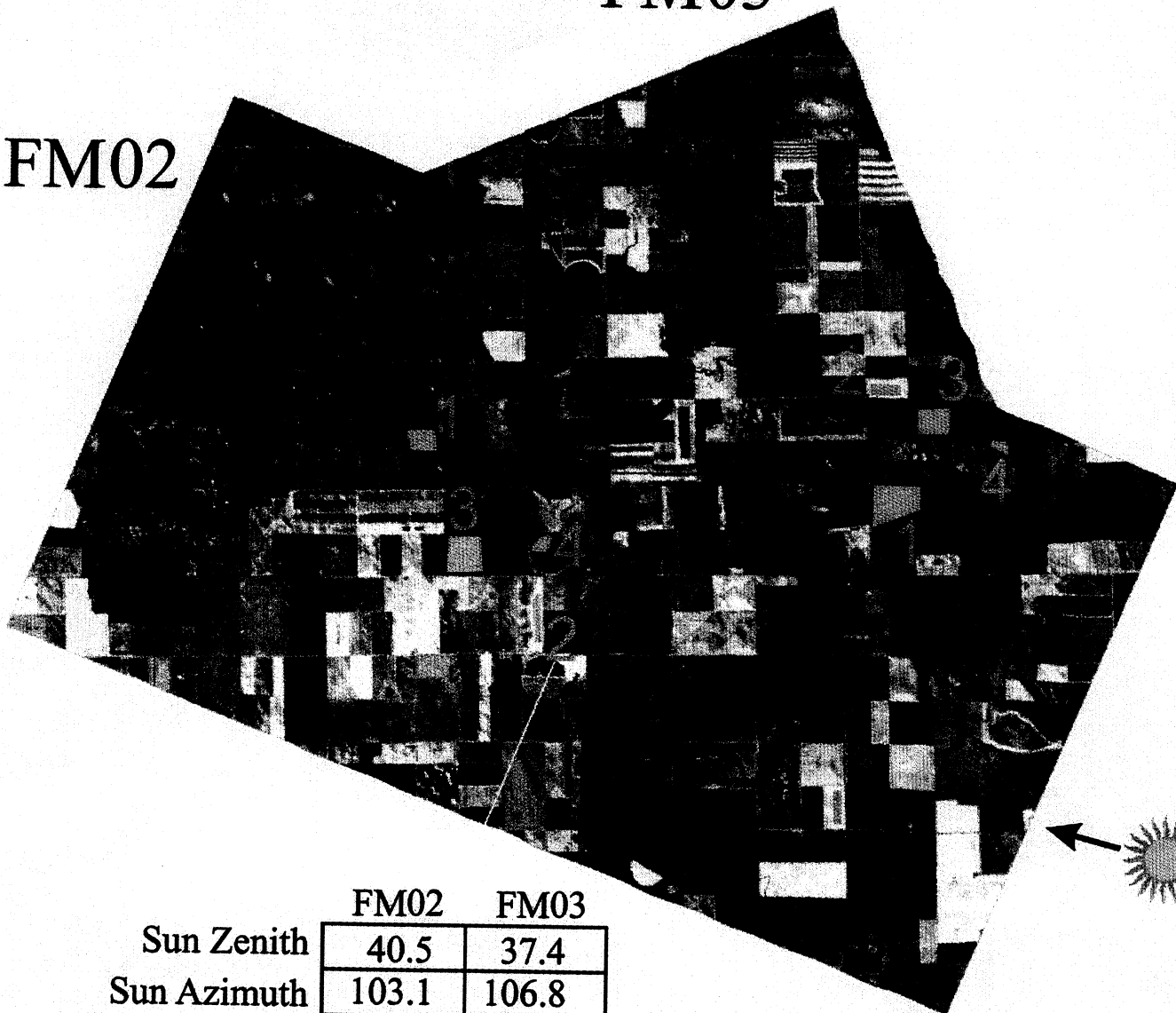






FM03

FM02



	FM02	FM03
Sun Zenith	40.5	37.4
Sun Azimuth	103.1	106.8

